DIMETHYL ETHER PRODUCTION FROM SYNTHESIS GAS WITH BIFUNCTIONAL CATALYST MIXTURES

A THESIS SUBMITTED TO
THE GRADUATE SCHOOL OF NATURAL AND APPLIED SCIENCES
OF
MIDDLE EAST TECHNICAL UNIVERSITY

BY

SALİH ERMİŞ

IN PARTIAL FULFILLMENT OF THE REQUIREMENTS
FOR
THE DEGREE OF MASTER OF SCIENCE
IN
CHEMICAL ENGINEERING

AUGUST 2022

Approval of the thesis:

DIMETHYL ETHER PRODUCTION FROM SYNTHESIS GAS WITH BIFUNCTIONAL CATALYST MIXTURES

submitted by **SALİH ERMİŞ** in partial fulfillment of the requirements for the degree of **Master of Science** i**n Chemical Engineering, Middle East Technical University** by,

Prof. Dr. Halil Kalıpçılar
Dean, Graduate School of **Natural and Applied Sciences** _____

Prof. Dr. Pınar Çalık
Head of the Department, **Chemical Engineering** _____

Prof. Dr. Naime Aslı Sezgi
Supervisor, **Chemical Engineering, METU** _____

Prof. Dr. Timur Doğu
Co-Supervisor, **Chemical Engineering, METU** _____

Examining Committee Members:

Prof. Dr. Suna Balcı
Chemical Engineering, Gazi University _____

Prof. Dr. Naime Aslı Sezgi
Chemical Engineering, METU _____

Assoc. Prof. Dr. Bahar İpek Torun
Chemical Engineering, METU _____

Asst. Prof. Dr. Harun Koku
Chemical Engineering, METU _____

Asst. Prof. Dr. Gökhan Çelik
Chemical Engineering, METU _____

Date: 24.08.2022

I hereby declare that all information in this document has been obtained and presented in accordance with academic rules and ethical conduct. I also declare that, as required by these rules and conduct, I have fully cited and referenced all material and results that are not original to this work.

Name Last name : Salih Ermiş

Signature :

ABSTRACT

DIMETHYL ETHER PRODUCTION FROM SYNTHESIS GAS WITH BIFUNCTIONAL CATALYST MIXTURES

Ermiş, Salih
Master of Science, Chemical Engineering
Supervisor: Prof. Dr. Naime Aslı Sezgi
Co-Supervisor: Prof. Dr. Timur Doğu

August 2022, 88 pages

In recent times, studies on alternative clean fuels have increased due to the depletion of crude oil reserves in the world because of increasing energy demand and the worldwide existence of severe air pollution. Dimethyl ether (DME) is, therefore, being investigated as an excellent clean fuel alternative in compression-ignition engines. DME can be produced from synthesis gas by two different methods, direct and indirect. Recently, the direct method has gained importance in the production of DME from syngas.

In direct DME synthesis from the syngas, methanol synthesis and methanol dehydration occur simultaneously in a bifunctional catalyst bed in the same reactor. Moreover, the thermodynamic limitations in the methanol synthesis stage are substantially overcome, resulting in a much higher yield and, thus, a significant improvement in the process economy.

Mesoporous silica aerogel support was synthesized. Silicotungstic acid (STA), tungstophosphoric acid (TPA), and both STA and alumina (Al) were loaded into this support using the impregnation method. Nitrogen physisorption technique, X-ray

diffractometer, Thermogravimetric analyzer, and Diffuse reflectance infrared Fourier transform spectroscopy were used to characterize the synthesized material.

According to thermodynamic analysis, operating pressure and temperature were selected 50 bar and 275 ℃, respectively. The CO/H_2 molar ratio was 1/1. Activity tests were performed under these conditions in a high pressure fixed bed reactor. All synthesized catalysts were physically mixed with the commercial methanol synthesis catalyst.

Sol-gel synthesis method was used to create silica aerogel support material that displayed Type IV isotherms with H3 type hysteresis loops, indicating mesoporous structure. The SA had a multipoint BET surface area of 793±14.1 m^2/g, BJH desorption average pore diameter of 10.9±0.4 nm, and BJH desorption cumulative pore volume of 3.44±0.09 cm^3/g. While the isotherm type remained the same, corresponding to Type IV, the metal loading into SA support changed the hysteresis loop to H1.

Physically mixed commercial methanol synthesis and commercial alumina catalysts were used for repeatability tests on DME production. DME selectivity was 50.9% in the commercial catalyst mixture.

It was observed that the DME selectivity increased with the increase of the amount of STA loaded on the SA support material from 10% to 35% by weight. The DRIFTS results demonstrate that increasing the amount of STA caused an increase in Brønsted acid sites, which also resulted in an increase in DME selectivity.

Among the synthesized catalysts, SA-35STA yielded the highest DME selectivity of 50.6% with the CO conversion of 66.1%. The highest DME yield in all synthesized catalysts was found to be 33.5% with the SA-35STA catalyst.

It was observed that SA-35STA together with MSC is a suitable catalyst candidate for direct DME synthesis.

Keywords: DME, Syngas, Silica Aerogel, STA, Bifunctional catalyst

ÖZ

ÇİFT FONKSİYONLU KATALİZÖR KARIŞIMLARI İLE SENTEZ GAZINDAN DİMETİL ETER ÜRETİMİ

Ermiş, Salih
Yüksek Lisans, Kimya Mühendisliği
Tez Yöneticisi: Prof. Dr. Naime Aslı Sezgi
Ortak Tez Yöneticisi: Prof. Dr. Timur Doğu

Ağustos 2022, 88 sayfa

Son zamanlarda artan enerji talebi nedeniyle dünyadaki ham petrol rezervlerinin tükenmesi ve dünya genelinde ciddi hava kirliliğinin olması nedeniyle alternatif temiz yakıtlar üzerine çalışmalar artmıştır. Dimetil eter (DME), bu nedenle, sıkıştırma ateşlemeli motorlarda mükemmel bir temiz yakıt alternatifi olarak araştırılmaktadır. DME sentez gazından doğrudan ve dolaylı olmak üzere iki farklı yöntemle üretilebilir. Son zamanlarda sentez gazından DME üretiminde doğrudan yöntem önem kazanmıştır.

Sentez gazından doğrudan DME sentezinde, metanol sentezi ve metanol dehidrasyonu aynı reaktördeki iki işlevli bir katalizör yatağında eşzamanlı olarak meydana gelir. Ayrıca, metanol sentezi aşamasındaki termodinamik sınırlamaların büyük ölçüde üstesinden gelinerek çok daha yüksek bir verim ve dolayısıyla süreç ekonomisinde önemli bir gelişme sağlanır.

Mezogözenekli silika aerojel desteği sentezlenmiştir. Silikotungstik asit (STA), tungstofosforik asit (TPA) ve hem STA hem de alümina (Al) emdirme yöntemi kullanılarak bu desteğe yüklenmiştir. Sentezlenen materyali karakterize etmek için

nitrojen fizyosorpsiyon tekniği, X-ışını kırınım ölçeri, Termogravimetrik analizör, ve dağınık yansıma kızılötesi Fourier dönüşüm spektroskopisi kullanılmıştır.

Termodinamik analize göre çalışma basıncı ve sıcaklığı sırasıyla 50 bar ve 275 ℃ seçilmiştir. CO/H_2 molar oranı 1/1'dir. Aktivite testleri bu koşullar altında yüksek basınçlı sabit yataklı bir reaktörde gerçekleştirilmiştir. Sentezlenen tüm katalizörler, ticari metanol sentez katalizörü ile fiziksel olarak karıştırılmıştır.

Sol-jel sentez yöntemi, mezogözenekli yapıyı gösteren H3 tipi histerezis döngüleri ile Tip IV izotermleri sergileyen silika aerojel destek malzemesini oluşturmak için kullanılmıştır. SA'nın çok noktalı BET yüzey alanı 793±14,1 m^2/g, BJH desorpsiyon ortalama gözenek çapı 10.9±0.4 nm ve BJH desorpsiyon kümülatif gözenek hacmi 3.44±0.09 cm^3/g'dır. Tip IV'e karşılık gelen izoterm tipi aynı kalırken, SA desteğine yüklenen metal histerezis döngüsünü H1 olarak değiştirmiştir.

DME üretimi üzerinde tekrarlanabilirlik testleri için fiziksel olarak karıştırılmış ticari metanol sentezi ve ticari alümina katalizörleri kullanılmıştır. DME seçiciliği, ticari katalizör karışımında %50,9'dur.

SA destek malzemesine yüklenen STA miktarının ağırlıkça %10'dan %35'e artmasıyla DME seçiciliğinin arttığı gözlenmiştir. DRIFTS sonuçları, STA miktarının arttırılmasının Brønsted asit bölgelerinde bir artışa neden olduğunu ve bunun da DME seçiciliğinde bir artışa neden olduğunu göstermektedir.

Sentezlenen katalizörler arasında SA-35STA, %66,1'lik CO dönüşümü ile %50,6'lık en yüksek DME seçiciliğini vermiştir. Sentezlenen tüm katalizörlerde en yüksek DME verimi SA-35STA katalizörü ile %33,5 olarak bulunmuştur.

SA-35STA'nın MSC ile birlikte doğrudan DME sentezi için uygun bir katalizör adayı olduğu gözlemlenmiştir.

Anahtar Kelimeler: DME, Sentez Gazı, Silika Aerojel, STA, İki işlevli katalizör

To my beloved family

ACKNOWLEDGMENTS

To begin with, I would like to express my sincere appreciation to my supervisor Prof. Dr. Naime Aslı Sezgi, for her endless contributions, patience, support, suggestions, and guidance every time. She always encouraged and helped me with her most profound knowledge. I would also like to express my deepest gratitude to my co-supervisor, Prof. Dr. Timur Doğu, for his guidance and endless support.

I would like to thank all of the professors of the Chemical Engineering Department for their encouragement, education, and wealth of knowledge about the chemical engineering discipline.

I am grateful to my dear lab-mates Seda Sivri and Merve Sarıyer for their patience, kindness, and help during the times I was in need. I would also like to express my gratitude to my former and current lab-mates Mehmetali İlker Şener, Arzu Arslan Bozdağ, Sohrab Nikazar, Abdul Rehman Habib, Sevil Göktürk, Çağla Bozcuoğlu, and Sümeyye Koçak Bütüner for their friendship and support. I also thank Dr. Birce Pekmezci Kahraman from Gazi University for her help.

I am also grateful to CZ-04 members Begüm Yılmaz and Selin Ernam for their support and endless friendship. Special thanks to Öznur Kavak for her support and help in difficult times. I thank my dear friends and colleagues, Ahmet Fırat Taşkın, Duygu Sezen Polat, Beste Avcı, Ezgi Altıntaş, Mehmet Soner Yaşar, Berkan Atman, Toprak Çağlar, Candan Karaeyvaz, Selin Karahan and Oğuz Ulaş Yaman for their endless friendship and help.

I wish to extend my special thanks to Türkay Rahman Arslanoğlu, Murat Oğuz Çolpankan, Fatih Tezer, Buğra Can Kesim, Ali Sinan Erçil and Ateş Batıkan Özdamar.

Many thanks to Mihrican Açıkgöz, Doğan Akkuş, and the entire METU Central Lab and Department of Chemical Engineering staff for the catalyst characterization

analysis. I would like to thank İsa Çağlar, Cemil Araçlı, Murat Akgün and Ramazan Küçükdanışman in particular for their assistance whenever I needed it.

Lastly, I would like to mention my dear family for bringing me to where I am today. Their unwavering faith in me and their support throughout my life shaped who I am. I want to express my gratitude to my dear mother, Ayşe Ermiş, for the sacrifices she made for me and her boundless love. I would also like to thank my dear father, Ömer Ermiş, for always being there for me whenever I needed him. They taught me essential life lessons. I would also like to thank my dear sister Saliha for always being there.

Finally, I would like to thank everyone who helped me complete this study, whether directly or indirectly.

TABLE OF CONTENTS

LIST OF TABLES

TABLES

LIST OF FIGURES

FIGURES

NOMENCLATURE

A_i : Area of component i in the GC pictogram

$n_{CO,0}$: Number of mole of CO fed to the reactor, mol

n_i : Number of moles of component i, mol

X_i : Fractional conversion of component i, %

S_i : Selectivity of component i, %

Y_i: Yield of component i, %

Abbreviations

BASF: Badische Anilin & Sodafabrik

BET: Branauer-Emmett-Teller

BJH: Barrett, Joyner, and Halenda

CA: Commercial alumina

CFC: Chlorofluorocarbon

CSA: Calcined silica aerogel

CZA: $CuO–ZnO–Al_2O_3$

DME: Dimethyl ether

DRIFTS: Diffuse reflectance infrared Fourier transform spectroscopy

EtOH: Ethanol

FA: Formic acid

FTIR: Fourier Transform Infrared Spectroscopy

GC: Gas chromatography

HPA: Heteropoly acid

LPG: Liquefied petroleum gas

MeOH: Methanol

MFC: Mass flow controller

MSC: Commercial methanol synthesis catalyst

SA: Silica aerogel

SAPOs: Silico-aluminophosphates

SFD: Supercritical fluid drying

STA: Silicotungstic acid

TCD: Thermal conductivity detector

TEOS: Tetraethyl-orthosilicate

TGA: Thermogravimetric analysis

TMCS: Trimethylchlorosilane

TMOS: Tetramethyl orthosilicate

TPA: Tungstophosphoric acid

WGSR: Water-gas shift reaction

XRD: X-Ray Diffraction

CHAPTER 1

INTRODUCTION

The rapid developments in technology and the rapid increase in the world population have caused the rapid consumption of petroleum resources and the increase in carbon emission with the use of these resources. This situation has led to more studies on developing new alternative fuels and environmentally friendly motor vehicle fuels from non-petroleum sources.

The most significant primary energy sources used as fuels worldwide are the traditional fossil resources like coal, crude oil, and natural gases. Nevertheless, fossil fuels produce CO_2, the primary source of global warming, and other poisonous gases such as SO_x and NO_x. Therefore, finding out renewable, sustainable, and environmentally friendly alternative fuels is critical for humankind to be used in heating, power, and transportation because of their low toxic gases compared to fossil fuels (Saravanan et al., 2017). By establishing goals to reduce carbon dioxide levels, European countries, including the UK, have recently made a commitment to reducing the harmful air pollution in their cities. In London, air pollution is a factor in 9400 deaths per year, and diesel vehicles are one of the main sources of air pollutants. As a result, the UK government declared its aim to outlaw diesel cars by the year 2040 in order to create a reliable, carbon-free transportation infrastructure (Shammut et al., 2019). However, only diesel cars will be banned, and the use of diesel in trucks, tractors and construction machinery will continue.

Over the last years, one of the trend topics has been searching for alternative energy resources to go through environmental crises and energy scarcity issues. Dimethyl ether (DME), produced from methanol dehydration or directly from syngas, is attracting significant interest as a clean alternative fuel due to increasing energy demand and its environmentally kindly feature in the 21st century (Li et al., 2020).

1.1 DME Properties and Applications

DME (CH_3OCH_3) is the most straightforward and secure ether, a non-toxic, non-carcinogenic, and non-corrosive chemical compound. Its boiling point is -24.9 ℃. It is a non-polluting high-efficiency compression ignition fuel owing to the autoignition characteristics of DME.

In the LPG business, DME can be used as a blend or independently as a substitute, according to the World LP Gas Association (WLPGA). Addition of 15–20 vol % DME to LPG will not affect on the current LPG infrastructure for storage, distribution, or use. China is the biggest DME manufacturer, using 90% of total DME production for LPG blending (Mondal & Yadav, 2019).

DME can be used as a fuel instead of traditional petroleum diesel because of its higher cetane number (55-60) and autoignition temperature (350 ℃), close to conventional diesel fuel. DME ignites without forming soot inside the diesel engine, similar to an oxygenated fuel additive, and improves the proper air/fuel mixture inside the engine. DME has lower carbon emissions than traditional compression-ignition engines' fuel owing to the absence of a C-C bond and high oxygen capacity (almost 35%). Burning of DME results in low NO_x (Hamed Bateni & Chad Able, 2019; Mondal & Yadav, 2019; Tokay et al., 2012).

Due to its low vapor pressure and chemical and physical stability properties, DME can be utilized as an aerosol propellant. Additionally, DME can substitute for chlorofluorocarbon (CFC), Freon, and R-134, leading to ozone layer depletion (Mondal & Yadav, 2019). DME is used as a raw material for chemicals like acetic acid, methyl acetate, light olefins, and aromatics (Mondal & Yadav, 2019). Table 1.1 demonstrates the DME properties. DME is a gas at ambient temperature and pressure. It liquefies at 5.9 bar and 25 ℃. As a result, this provides safe storage and handling (Peinado et al., 2020). In addition to this, because of the similar physical properties of DME and LPG, there is no need for new technology for handling and

safety procedures. LPG cylinder can be used to store the liquid DME. This provides an economic advantage (Sorenson, 2001).

Table 1.1 DME properties (Mondal & Yadav, 2019)

Chemical formula	CH_3OCH_3
Molecular weight (g/mol)	46.07
Boiling point (°C)	-24.9
Vapor pressure (atm at 20 °C)	5.1
Liquid density (g/cm^3 at 20 °C)	0.67
Specific gravity (25 °C/4 °C)	0.661
Cetane number	55-60
Flammability Limits in the air (vol%)	3.4-17
Calorific value LHV (kcal/kg)	6925

1.2 Production Methods of DME

DME is produced in two different methods. First, DME is manufactured by a traditional two-step process, indirect method, which includes methanol production from syngas (R1 and R2 below) via a Cu-ZnO-based catalyst and then dehydration to DME (R3) on a solid acid catalyst in a separate reactor. Syngas for the methanol synthesis step is produced from fossil sources such as natural gas, coal, and oil (Bayat & Dogu, 2016). Steam/dry reforming of natural gas, autothermal reforming of methane, catalytic partial oxidation of methane are production method of syngas (Rostrup-Nielsen, 2000). Recently, the use of biomass-derived syngas via gasification has received significant attention. The conversion of syngas to methanol is limited by thermodynamic equilibrium, which needs high pressures and low temperatures to achieve conceivable per-pass conversions in the traditional process (Bayat & Dogu, 2016).

The second method is direct DME synthesis from syngas, in which methanol synthesis (R1 and R2) and methanol dehydration (R3) are triggered simultaneously

in a bifunctional catalyst bed in the same reactor. This method has received much attention because of its thermodynamical and economic benefits. Figure 1.1. shows these two methods to produce DME.

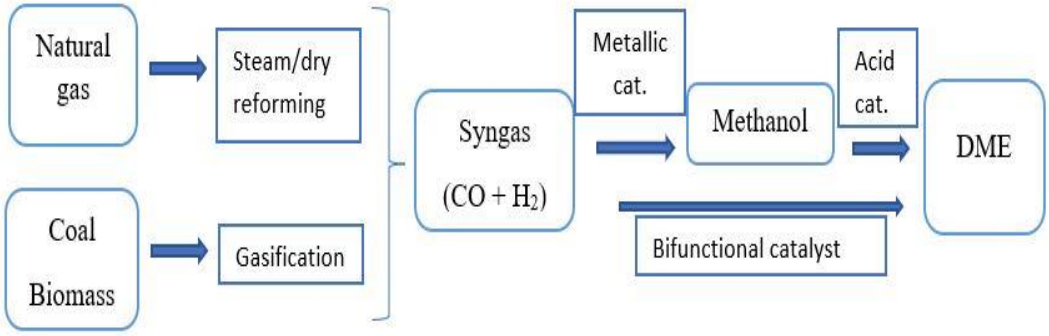

Figure 1.1. Possible schematic representations for the production of DME (Saravanan et al., 2017)

The critical reactions in DME synthesis are the hydrogenation of CO and CO_2 to methanol (R1 and R2), methanol dehydration to DME (R3), and water-gas shift reaction (WGSR) (R4) as a side reaction (Bayat & Dogu, 2016; García-Trenco & Martínez, 2012).

$CO + 2H_2 \rightleftharpoons CH_3OH$ (R1)

$CO_2 + 3H_2 \rightleftharpoons CH_3OH + H_2O$ (R2)

$2CH_3OH \rightleftharpoons CH_3OCH_3 + H_2O$ (R3)

$H_2O + CO \rightleftharpoons H_2 + CO_2$ (R4)

The overall stoichiometry of DME synthesis from syngas, including a mixture of CO and H_2, can be expressed as (R5) and (R6). As a result of the simultaneous occurrence of the (R1) and (R3) reactions, the net (R5) reaction occurs. However, in the direct method, not only the (R1) and (R3) reactions but also (R4) reaction can simultaneously occur. As a result, (R6) reaction gives the overall net reaction in the direct synthesis of DME (Bayat & Dogu, 2016; Saravanan et al., 2017):

$2CO + 4H_2 \rightleftharpoons CH_3OCH_3 + H_2O$ (R5)

$3CO + 3H_2 \rightleftharpoons CH_3OCH_3 + CO_2$ (R6)

In the second method, the methanol formed from the (R1) and (R2) reactions is consumed through the (R3) reaction, shifting the chemical equilibrium for the (R1) and (R2) reactions to the righthand side. It allows high CO or CO_2 conversion. The water formed from the (R2) and (R3) reactions also reacts with CO to produce CO_2 and H_2 (WGSR, R4), which are the reactants of the methanol synthesis (García-Trenco & Martínez, 2012).

In the DME production, due to highly exothermic reactions, they are notably restricted via the thermodynamic equilibrium. Nonetheless, direct DME production from syngas has more benefits than indirect (Celik et al., 2013). Furthermore, it is more cost-effective than the indirect method due to the use of a single reactor without purification and methanol transport units (Saravanan et al., 2017).

CHAPTER 2

CATALYSTS FOR DME SYNTHESIS

Extensive research is being done to find better catalysts with higher selectivity towards DME formation and a lower tendency to produce hydrocarbons and coke. Catalysts for the syngas to DME process are bifunctional catalysts consisting of a metallic function for synthesizing methanol and a solid acid function for converting methanol to DME in the direct method (Azizi et al., 2014).

The catalysts' primary goal is to reduce the activation energy of the reaction. Catalytic activity, product selectivity, and stability are crucial parameters in catalyst selection. To catalyze the reaction, catalysts typically have a porous structure and catalytically active sites on their surface. Many phenomena such as adsorption/desorption, diffusion, and reactant species interaction to these active sites may occur during the reactions.

2.1 Methanol Synthesis Catalysts

For methanol synthesis in the direct method, metallic catalysts are required for the CO hydrogenation reaction to produce methanol. The metallic function chiefly consists of oxides such as CuO and ZnO. The most widely used metallic catalyst is the copper-based catalyst for methanol synthesis. Converting syngas to methanol relies on the copper metal surface area. ZnO plays a crucial role in keeping the active copper metal in optimum distribution, therefore supplying many active sites subjected to gaseous reactants. Metallic copper clusters are the active sites for methanol synthesis reaction and WGSR in CuO–ZnO–Al_2O_3 catalysts (Azizi et al., 2014). Al_2O_3 is a well-known third component that is frequently utilized in a Cu-based catalyst since it is an effective promoter. Because of its disorderly and defective surface domain, it cannot only generate zinc aluminate to stop the

aggregation of active sites but also speeds up the adsorption and activation of CO. The extremely scattered Cu/ZnO structure can also be stabilized by it (Ali et al., 2015; Liu et al., 2003).

The first traditional catalyst to convert syngas to methanol was developed by Badische Anilin & Sodafabrik (BASF) in 1923 using a $ZnO\text{-}Cr_2O_3$ catalyst, which has an operating temperature between 350 and 400 ℃ and operating pressure between 240 and 350 bar. Nevertheless, impurities such as sulfur and chlorine in syngas poison the catalyst (Saravanan et al., 2017).

The ability for Imperial Chemical Industries (ICI) to use the more active Cu/ZnO catalyst was made possible in the 1960s by the creation of a synthesis gas free of sulfur. This catalyst may function at significantly lower temperatures and pressures, specifically 60-80 bar and 250-280 ℃, because of its high activity. Due to these improvements, the compression and heat exchange workload in the recycling loop was significantly reduced. Because the co-production of light hydrocarbons was essentially suppressed at the lower reaction temperature, selectivity was also enhanced (Lange, 2001).

Due to zirconia's strength, thermal resistance, and excellent stability, it can also be employed as a support in place of zinc oxide. Zirconium oxide is a superior support than others and offers homogeneous dispersion of CuO on ZrO_2 surface, potentially enhancing the catalyst's catalytic activity. Because of its strong acid-base properties, porous structure, and thermal stability, SiO_2 could also be utilized as a catalyst support. However, catalysts with silica support have very low methanol selectivity and are essentially inert for methanol synthesis. As a result, additional metal oxides could also be used as a promoter to increase the catalyst's catalytic activity when added to the silica support (Liu et al., 2003).

2.2 Methanol Dehydration Catalysts

For methanol dehydration, acidic catalysts are needed to convert methanol to DME in the direct method. It is well known that the surface of the solid-acid catalysts has either Brønsted or Lewis-acid type (Azizi et al., 2014). Different catalysts, consisting of heteropoly acids (HPAs), silico-aluminophosphates (SAPOs), aluminosilicates, and ion exchange resins, bulk and modified γ-Al_2O_3, and bulk and modified HZSM-5, are used for dehydration of methanol. However, efforts are still being made to identify a suitable catalyst that possesses desirable characteristics such as satisfactory stability, proper acidity, high activity, hydrophobic surface, high selectivity toward DME, and low production (and recovery) costs (Hamed Bateni & Chad Able, 2019).

γ-Al_2O_3 is a catalyst for the dehydration of methanol. Due to its low cost, high surface area, great thermal and mechanical stability, high mechanical resistance, and high selectivity for DME, it is particularly appealing. Furthermore, because it contains few extremely acidic sites, mostly Lewis acid sites, it has strong catalytic activity toward DME production. Although γ-Al_2O_3 is active, it tends to significantly adsorb water hence reducing activity (Azizi et al., 2014).

Zeolites are crystalline aluminosilicates with periodic cage and channel arrangements that are used extensively in industry as catalysts, adsorbents, and ion exchangers. From the literature, it can be concluded that zeolite materials can function as a solid-acid catalyst in the methanol dehydration process at temperatures between 250 and 400 °C and pressures up to 18 bar. Zeolites generally have a high surface area compared to other catalysts because of their microporous crystalline interface. However, DME might be prevented from rapidly diffusing through the pores by the zeolites' narrow and slender microporous structure. As a result, by-product production and carbonaceous chemical deposition could cause zeolites to rapidly lose their catalytic activity and selectivity (Azizi et al., 2014).

Beta zeolite cores and polycrystalline Y zeolite shells (BFZ) is another efficient methanol dehydration catalyst. Because of its mesoporosity and moderate acid strength, BFZ in the H-form (HBFZ) has a high activity for CO hydrogenation (Wang et al., 2013).

Due to its decreased coke deposition, lower by-product generation, and improved water resistance, aluminum phosphate ($AlPO_4$) is also a suitable catalyst in the synthesis of DME. Al/P molar ratio, production technique, and activation temperature are observed to affect $AlPO_4$'s catalytic activity in the dehydration of methanol (Siva Kumar et al., 2006; Yaripour et al., 2005).

2.2.1 Heteropoly Acids

Heteropoly acids (HPAs) are strong acidic catalysts with Brønsted acidity and, in some cases, even higher than traditional solid catalysts. HPAs have various molecular structures, which are Keggin and Dawson. HPAs are more common structures for catalytic applications. The Keggin type HPAs are represented as $H_{8-n}[X^{n+}M_{12}O_{40}]$, in which X is the heteroatom like Al^{3+}, P^{5+}, and Si^{4+}, n is the oxidation state, and M is the metal ion such as W^{6+} and Mo^{6+}. On the other hand, the Dawson ions of HPAs are represented as $[X^{(n)}{}_2M_{18}O_{62}{}^{2(8-n)-}]$, where X is Si, Ge, P, and S, and M is W and Mo (Jansen et al., 1997). The HPAs heteroatom has a highly acidic Brønsted acid site. Therefore, compared to zeolites, HPA performs better at lower reaction temperatures. HPAs typically have a low surface area, which can be increased using proper support. Further research has demonstrated the beneficial effect of mesoporous silicate structures as a support for HPAs during the dehydration reaction. Silicotungstic acid (STA) and tungstophosphoric acid (TPA) are the most common HPAs (Hamed Bateni & Chad Able, 2019; Mondal & Yadav, 2019).

Keggin-type HPA catalysts have been widely used for alcohol dehydration, mainly ethanol and methanol (Hamed Bateni & Chad Able, 2019). HPAs have very high solubility in polar solvents. Methanol dehydration reaction over Keggin type HPA

clusters with various heteroatoms (X=P^{5+}, Si^{4+}, Al^{3+}, and Co^{2+}) and proposed an associative reaction pathway. Using the wet impregnation method, the Keggin type TPA and STA were well-deposited on various catalyst supports, including titania-based, silica-based, ZrO_2, and Nb_2O_5 (Hamed Bateni & Chad Able, 2019). With the exception of 15% TPA/TiO_2, which had a surface area of 45 m^2/g, the supported HPAs had a BET surface area of more than 100 m^2/g. It is worth noting that the HPAs supported on SiO_2 had a higher BET surface area (over 200 m^2/g). The support was found to affect the acid strength of the catalysts in the order SiO_2 > TiO_2 > Nb_2O_5 > ZrO_2 simply by increasing the interaction between the HPAs and the support (Hamed Bateni & Chad Able, 2019; Mondal & Yadav, 2019).

Although the acid strength of TPA is higher than that of STA, TPA's main disadvantage is its extremely low surface area and almost nonporous structure (Sener, 2019; Varıslı, 2007).

To increase the surface area for heterogeneous catalytic applications, STA must be incorporated into a suitable support material such as silica aerogel, SBA, MCM-41 and zeolites.

2.3 Silica Aerogel

Porous materials are useful in various applications, including adsorption, sensing, and catalysis. They are ideal for these applications due to their high surface areas, porosities, adjustable frameworks, and surface properties. The hydrogenation reaction can occasionally be catalyzed using porous materials. Without adding additional catalyst, porous materials typically offer catalytically active locations to activate the hydrogen source in the ways listed below: a) acidic/basic sites exposed at the surface of porous metal oxides; b) metal ions or cluster nodes and the terminal ligands in metal-organic polymers. Due to their high surface area and different synthesis methods, porous materials have emerged as one of the most crucial substitutes for noble-metal catalysts. Additionally, compared to a metal-based

catalyst, this porous metal-free catalyst system would result in a lower cost, a more uniform distribution of active sites, and improved stability. (Su & Chen, 2017).

Aerogels are solid porous materials with small pore sizes, high specific surface areas, and good optical transmission. Silica aerogels have become quite popular since they have unusual properties like a high specific surface area (500-1200 m^2/g), a high porosity (80-99.8 %), a low density (0.003 g/cm^3), a high thermal insulation value (~0.01 W/mK), an ultra-low dielectric constant (k = 1.0-2.0), and a low index of refraction (1.05). The pore size range from 5 to 100 nm, and the average pore diameter range from 10 nm to 40 nm (Gurav et al., 2010).

There are several use areas for aerogels, such as sensors, thermal insulation, electronic devices, capacitors, imaging devices, catalysts, pesticides, and cosmic dust collection (Gurav et al., 2010; Soleimani Dorcheh & Abbasi, 2008). Recently, several groups have started working in the field of silica aerogels.

2.3.1 Synthesis of Silica Aerogel

Sol-gel processing is a popular and dependable method for producing materials, mainly metal oxides with uniform, small particle sizes and varied morphologies. It entails converting a system from a liquid sol phase to a solid gel phase. The synthesis of silica aerogel can be divided into three general steps:

a. Gel preparation: A sol-gel method is used to create the silica gel. The sol is prepared with a silica source solution, and gelation forms with the addition of the catalyst. The dispersion media used to create the gels is typically used to categorize them; examples include hydrogel, alcogel, and aerogel (for water, alcohol, and air, respectively).
b. Aging of the gel: In the first phase, the produced gel is aged in its mother solution, prepared in the first step. The gel becomes stronger during this aging process, minimizing shrinkage during the drying process.

c. Drying of the gel: The gel should be clear of pore fluid at this step. To prevent the gel structure from collapsing, drying is carried out under specific circumstances which are freeze-drying, evaporation and supercritical fluid drying (Soleimani Dorcheh & Abbasi, 2008).

2.3.1.1 Gel Preparation

Low temperature sol-gel processing creates an inorganic network from a solution or creates an amorphous network to prevent crystallization. The term "sol-gel process" refers to the transition from a colloidal solution (liquid) to a bi- or multiphase gel (solid) and is what makes this reaction unique. Figure 2.1 illustrates the schematic depiction of the conventional sol-gel process.

Generally speaking, silica nanostructured solids are made by the hydrolysis and condensation of silica precursor molecules, which results in the formation of siloxane bridges (Si-O-Si). Due to the recent rapid advancement of sol-gel chemistry, silicon alkoxides are now used as precursors in most silica aerogel production processes. The most common silicon alkoxides are tetramethyl orthosilicate (TMOS, $Si(OCH_3)_4$) and tetraethyl-orthosilicate (TEOS, $Si(OCH_2CH_3)_4$), with the typical chemical formula $Si(OR)_4$ giving rise to aerogels called Silica (Gurav et al., 2010; Maleki et al., 2014).

The hydrolysis of silicon alkoxides is a versatile technique that can produce various materials depending on the parameters and acid or base catalyst used. The Si/H_2O ratio is critical. The proportions of TMOS (or TEOS) and water, on the other hand, are essential and result in different products. A third solvent is needed to homogenize the mixture since water and alkoxysilanes like TEOS and TMOS are only partially miscible. Solvents utilized for this purpose include alcohols, acetone, dioxane, and tetrahydrofuran, to name a few. Alcohols can engage in an esterification reaction, which lowers the rate of hydrolysis even if they are utilized as solvents. To approach complete alkoxide hydrolysis, the molar ratio of $H_2O/Si(OR)_4$ in the sol should be at

least 2/1. Chemical reactions are accelerated, and gelation times are reduced as water concentration increases.

During the hydrolysis step, the following reaction takes place:

$$Si(OR)_4 + H_2O \rightarrow HO - Si(OR)_3 + ROH$$

When the hydrolysis reaction is complete, the above reaction becomes

$$Si(OR)_4 + 4H_2O \rightarrow Si(OH)_4 + 4ROH$$

where R = vinyl, alkyl, or aryl groups.

The resulting silanol groups form siloxane bridges (Si-O-Si). They can react with each other or alkoxides (Si-OR) by giving water or alcohol. Condensation usually occurs in the presence of alcohols and essential catalysts (Gurav et al., 2010).

Water condensation:

$$(\mathrm{OR})_3\mathrm{Si} - \mathrm{OH} + \mathrm{HO} - \mathrm{Si}(\mathrm{OR})_3 \rightarrow (\mathrm{OR})_3\mathrm{Si} - \mathrm{O} - \mathrm{Si}(\mathrm{OR})_3 + \mathrm{H_2O}$$

Alcohol condensation:

$$(\mathrm{OR})_3\mathrm{Si} - \mathrm{OR} + \mathrm{HO} - \mathrm{Si}(\mathrm{OR})_3 \rightarrow (\mathrm{OR})_3\mathrm{Si} - \mathrm{O} - \mathrm{Si}(\mathrm{OR})_3 + R\mathrm{OH}$$

An Si-O-Si network develops following the hydrolysis and condensation events that produce the gel.

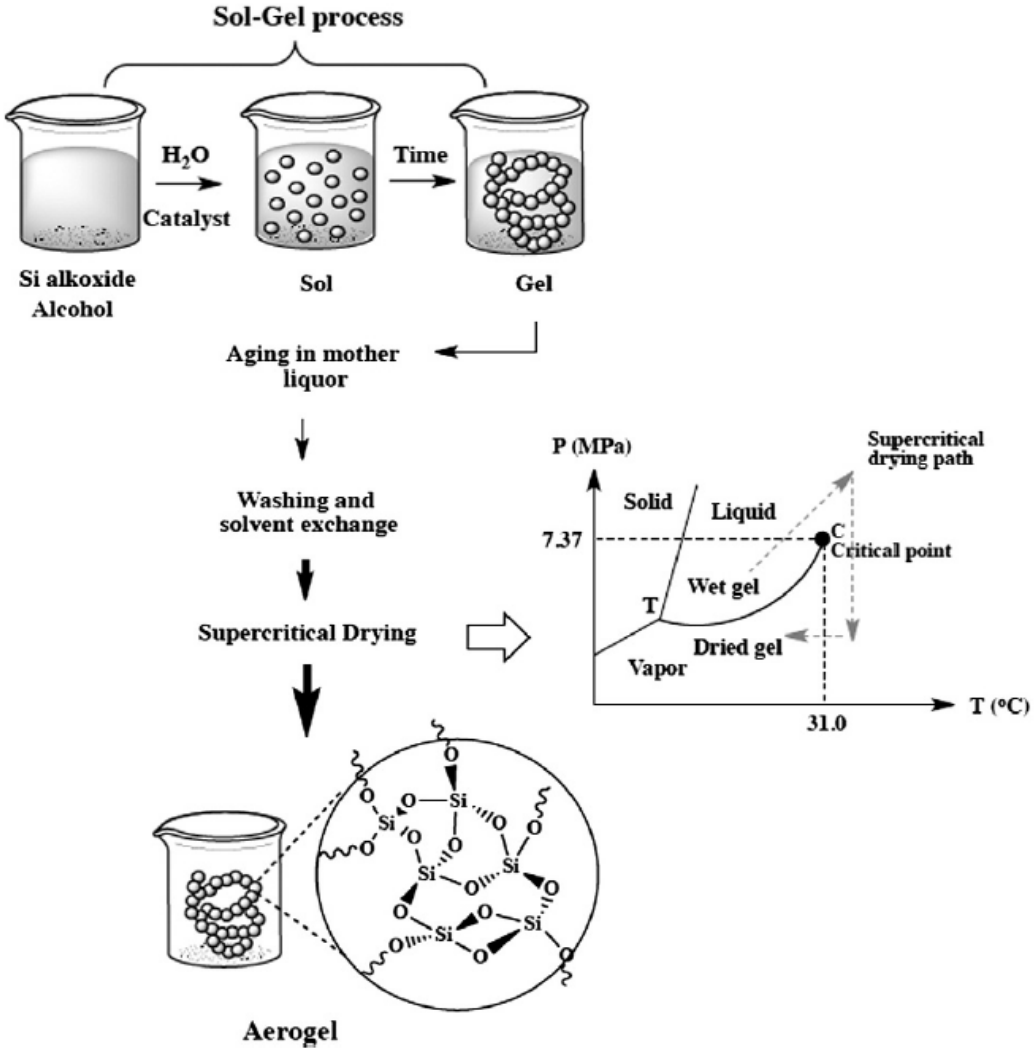

Figure 2.1. The schematic representation of the typical sol-gel method (Maleki et al., 2014)

A catalyst is used to perform hydrolysis. Three procedures are suggested: acid catalysis, base catalysis, and two-step catalysis. Acid catalysis is carried out with HCl, H_2SO_4, HNO_3, HF, oxalic acid, formic acid, and acetic acid. Base catalysis usually includes diluting ammonia 10^{-2} M (Soleimani Dorcheh & Abbasi, 2008). In the last procedure, TEOS, ethanol, oxalic acid, and water were combined in the first stage in the following molar ratios: $1:8:6.23x10^{-5}:3.75$. A mixture of H_2O and NH_4OH in the molar ratio of $2.25:4x10^{-2}$, respectively, was added to the silica sol in the second step (prepared in the first step). The rate of condensation processes can

be accelerated and the gelation duration decreased by adding NH_4OH as a second catalyst to a solution that was previously catalyzed by HCl (Rao et al., 2005).

In general, acid-catalyzed hydrolysis and condensation result in weakly branched and microporous structures, while basic conditions or two-step acid-base treatments increase crosslinking, resulting in less microporosity and a more even distribution of larger pores in silica gels (Soleimani Dorcheh & Abbasi, 2008).

2.3.1.2 Aging of the Gel

Aging mechanisms can affect the structure and properties of the gel. The two mechanisms are:

(a) Silica dissolved from the surface of the particle and reprecipitated onto the necks between the particles, causing neck development. (b) Dissolution of smaller particles and precipitation onto larger ones. These two mechanisms operate simultaneously but at a different rate (Soleimani Dorcheh & Abbasi, 2008).

The final silica aerogels get stronger and develop mechanically stronger inorganic networks as a result of wet-gel aging (Maleki et al., 2014; Soleimani Dorcheh & Abbasi, 2008). The gel is strengthened during this aging process so that drying causes less shrinking. The process is finished by leaving the gel in the solvent once it has gelled. The result of the reaction is the aerogel product (Thapliyal & Singh, 2014).

By silica's dissolution reprecipitation process, washing in water and ethanol improves the solid portion of the gel's liquid permeability. By introducing new monomers to the silica network and increasing the degree of siloxane cross linking, aging in a siloxane solution increases the stiffness and strength of the alcogel; on the other hand, this process will decrease the permeability. Material is moved to the neck region between particles as the gel network ages, making it more stiff (Soleimani Dorcheh & Abbasi, 2008).

After the aging period, a solvent exchange method can be applied to avoid capillary stress. The water at the pores can be replaced by hexane.

2.3.1.3 Drying of the Gel

After gel formation, hydrolysis and condensation events result in the development of a Si-O-Si network. Aging is the process of making the gel network stronger, and it may involve further sol particle condensation, dissolution, and reprecipitation as well as phase changes in the solid or liquid states. A porous solid that retains the solvent is created through aging. Drying removes most of the gel's solvents (primarily alcohol and water in the case of an alkoxide-derived gel). The capillary forces created in the fine pores by the liquid-vapor interfaces cause cracking of the gel web during the drying process. Therefore, drying the gel is a significant step. Drying is managed by capillary pressure. During drying, capillary tension can increase to 100–200 MPa. The gradient brings on mechanical harm in capillary pressure within the pores.

Three main methods of drying are commonly used: (1) freeze-drying, in which the solvent inside the pores must cross the liquid-solid and then the solid-gas equilibrium curves; (2) evaporation, which implies crossing the solvent's liquid-gas equilibrium curve; and (3) supercritical fluid drying (SFD), in which the supercritical condition is achieved without crossing the solvent's equilibrium curve.

The freeze-drying method generally freezes the solvent in the pores before sublimating it under a vacuum. The resulting substance is referred to as a cryogel. However, this procedure results in silica products with large pores that are fractured or powder-like because the solvent crystallizes within the pores. Nonetheless, this issue can be mitigated using solvents with low expansion coefficients, high sublimation pressures, and rapid freezing in liquid nitrogen at cooling rates greater than 10 Ks^{-1}.

Evaporation without specific surface treatments often results in dense and cracked materials called xerogels. Densification during evaporation results from the condensation of the residual reactive silica species. Because silica chains are naturally flexible, when wet silica gel is subjected to capillary pressure, the previously dispersed surface hydroxyl/alkoxy groups react and create new siloxane bonds, leading to irreversible shrinkage. Furthermore, compared to aerogels of the same composition, the pore structures of xerogels frequently collapse. A large capillary pressure gradient forms inside the porous structure during drying as a result of the varied pore sizes present in the gel, causing mechanical damage.

Strengthening the gel to withstand capillary strains is one solution. This can be accomplished by replacing some of the siloxane (Si-O-Si) bonds with flexible and non-hydrolyzable organic bonds (Si-R) created by using organosilanes as precursors to create the aerogel network. The organic group will allow the aerogel to return to its original wet gel size without causing any cracks within the gel. Other methods include changing the capillary force experienced by the network by surface modification of the silica with alkyl groups and providing a surface devoid of Si-OH groups. Using low surface tension solvents or adding additives to regulate the drying process are two other strategies for overcoming generated capillary pressures. Surface tension and capillary pressure are directly correlated, so when a low surface tension solvent is evaporated from a wet silica gel network, it results in lower capillary pressure than when alcohol is evaporated.

In supercritical drying method, gel is dried at a critical point to eliminate the capillary forces. The liquid in the pores is removed when it is above its critical temperature (T_c) and pressure (P_c), i.e., when it is in the supercritical state. There are no liquid-vapor interfaces in this condition. Therefore, no capillary pressure gradients exist. The supercritical fluid drying method can be carried out in two ways: by extracting the synthesis solvent (1) with supercritical organic solvents (common organic alcohol solvent such as ethanol and methanol at about 260 °C), which is known as the hot process and (2) with supercritical CO_2 at a temperature slightly above the

critical temperature of CO_2 (31 °C), which is known as the cold process (Gurav et al., 2010; Maleki et al., 2014; Soleimani Dorcheh & Abbasi, 2008).

Surface modification is a critical step in silica aerogel's ambient pressure drying preparation. There are numerous silylating reagents available for surface modification. Among these have been reported phenyltrimethoxysilane (PTMS), phenyltriethoxysilane (PTES), ethyltriethoxysilane (ETES), trimethylchlorosilane (TMCS). In general, the surface modification of silica alcogel is dominated by the reaction described below (Wu et al., 2011).

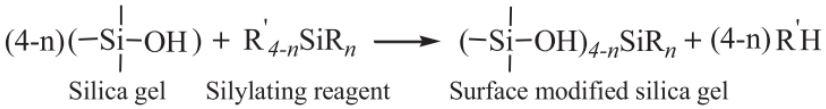

where R is alkyl, aryl phenyl, or vinyl group; R' is alkoxy or halogen group.

The most often utilized and well studied surface modification agent is TMCS. The most prevalent functional group on the interior pore surface of silica gels is the hydroxyl group (-OH). It was proposed that as the modification progressed, the -OH group reacted with the Cl^- in TMCS to form HCl, and then the $-OSi(CH_3)_3$ functional group was attached to the silica gel surface. The hydrophilic nature of the silica network's internal surface was converted to hydrophobic. On the other hand, silylating reagent concentrations were diluted using alcohols and low surface tension n-Hexane solvents to slow down the rate at which they reacted during the surface modification procedure. However, the surface modification method has been well discussed before. The reaction mechanism of silica alcogel and TMCS is demonstrated by the following reaction (Wu et al., 2011).

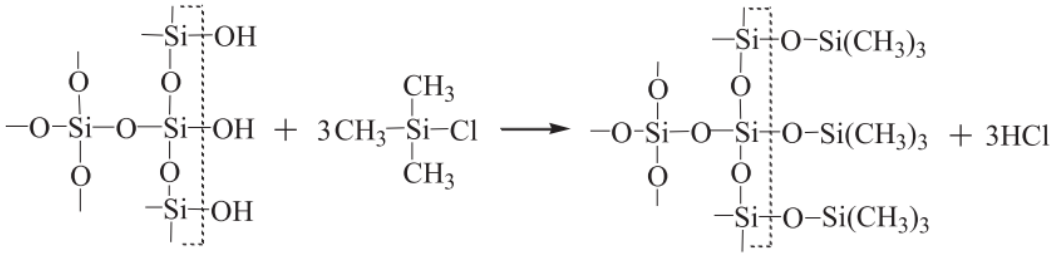

Silica alcogel TMCS Modified silica gel

The reaction of TMCS with water inside the pores take place simultaneously, as represented by the following reaction.

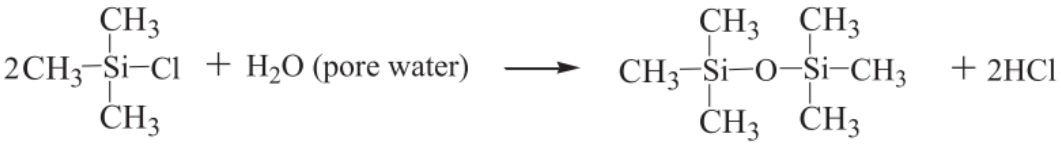

In order to lower capillary pressure into the pores, water is then replaced with the low surface tension solvent n-hexane. Simultaneously, the hexamethyldisiloxane ($(CH_3)_3Si\text{-}O\text{-}Si(CH_3)_3$) formed would adsorb on the surface, enhancing the expulsion of alcohols/H_2O/HCl phase and the entrance of n-hexane due to the incompatibility between hexamethyldisiloxane/n-Hexane phase and alcohols/H_2O/HCl phase, and ultimately (Wu et al., 2011).

2.4 Catalysts and Operating Conditions for DME Synthesis

One of the most important parameters influencing reaction performance is the catalyst. Commercial $Cu/ZnO/Al_2O_3$ and $\gamma\text{-}Al_2O_3$ solid catalysts are generally preferred for methanol synthesis and dehydration, respectively. The following are examples of catalysts used in the synthesis of DME found in the literature:

Bifunctional hybrid catalysts were investigated based on phosphotungstic acid ($H_3PW_{12}O_{40}$, HPW) supported on TiO_2 combined with Cu-ZnO(Al) catalysts. Activity experiments were conducted in a fixed-bed reactor filled with 0.225 g of hybrid catalysts. With a molar composition of 4.5% CO_2, 22.0% CO, 58.8% H_2, and

14.7% N_2, the syngas mixture had a flow rate of 75 NmL/min. The catalytic behavior of CZA-xHPW/Ti hybrid catalysts for direct DME synthesis from syngas (30 bar and 250℃) is affected by the amount of HPW loaded. The methanol yield on CZA-HPW/Ti hybrids was always lower than the methanol yield on the Cu-ZnO(Al) catalyst. Only hybrids with HPW loading above 1.7 monolayers are effective for direct DME synthesis. The highest selectivity for DME was obtained with the 2.7 monolayer hybrid (CZA-2.7HPW/Ti). The DME selectivity in the 2.7 monolayer hybrid was 53.0% (Millán et al., 2020).

The catalytic conversion of syngas to DME was investigated on a novel Cu-loaded STA-UiO catalyst. Because of its exceptional stability and porosity, a Zr-MOF (UiO-66) called the Zr-Metal-organic framework, was chosen as the catalyst host and support. UiO-66 was functionalized with silicotungstic acid ($H_4SiW_{12}O_{40}$, STA) in a one-pot synthesis method before being loaded with Cu using a simple solid grinding method. Gas mixtures of H_2/CO (2/1), with 50% N_2 as the internal calibration standard were fed to the reactor. Catalysts were tested at 290 ℃, 3.0 MPa, and 3000 ml/g_{cat}.h. Cu/STA-UiO has a DME selectivity of 69.3%, which is significantly higher than Cu/UiO-66, Cu-ZnO/γ-Al_2O_3, and Cu/γ-Al_2O_3. Cu/STA-UiO has a CO conversion of 1.99%. The higher DME selectivity of Cu/STA-UiO is explained by the increased Brønsted acid sites and the proximity between Cu atoms and STA molecules (Li et al., 2020).

Methanol synthesis catalysts with different Cu/Zn/Al or Cu/Zn/Zr molar ratios were used as the metallic catalyst for methanol production. STA and TPA, which were impregnated into these methanol synthesis catalysts, have been investigated for synthesizing DME in a fixed bed stainless-steel tubular reactor at different reaction pressures (30-50 bars) and different reaction temperatures (200-300 °C). The feed flow rate was 50 ml/min with a CO/H_2 molar ratio of 1/1 and a space-time of 0.72 s.g/ml. In this study, the new bifunctional CZA:631 catalysts (composed of 60% Cu, 30% Zn and 10% Al in molar) impregnated with 25% and 30% STA by weight produced exceptionally high DME selectivity values of 59.1% and 63.1%,

respectively, and high CO conversion values of 28% and 39%, respectively, at 275 °C and 50 bar (Pekmezci Karaman et al., 2020).

The direct synthesis of DME over a commercial HifuelR-120 and TPA impregnated HZSM-5 catalysts was investigated at a reaction temperature of 200-300 °C and a reaction pressure of 50 bar in a fixed bed stainless-steel tubular reactor. The feed flow rate was 50 ml/min with a CO/H_2 molar ratio of 1/1. With 46% CO conversion at 275 °C and 50 bar, a maximum DME selectivity of approximately 57% was achieved (Pekmezci Karaman & Oktar, 2020).

The bifunctional Cu/Al_2O_3 catalysts were investigated with the syngas ($H_2/CO = 2$) at 5 MPa with a gas hourly space velocity (GHSV) of 1500 mL/($h.g_{cat}$) and a temperature range of 260–320 °C. As reaction temperature rises from 260 °C to 320 °C, CO conversion increases from 32.6% to 73.5%, while DME selectivity decreases from 65.8% to 46.5% over Cu/Al_2O_3 with a 10% copper molar ratio. The extensively scattered Cu and Cu embedded into the alumina matrix that prevents Cu from sintering at the high reaction temperature may be due to the CO conversion continuing to increase even at 320 °C. However, DME selectivity fell from 65.8% to 46.55% as reaction temperature increased. The fact that a portion of DME is hydrocracked to hydrocarbons at 320 °C may be due to the sharp rise in hydrocarbon selectivity (Wang et al., 2016).

Bifunctional copper-zeolite catalysts were used for the DME synthesis reaction in a fixed-bed stainless steel tube reactor. A typical catalyst loading was 0.5 g, and the feed H_2/CO molar ratio was 2. The reaction was conducted at 260 °C with a gas hourly space velocity (GHSV) of 3600 $cm^3/g/h$ and a pressure of 20 bar maintained with a back pressure regulator. The maximum DME selectivity and the CO conversion of the Cu-ZnO-Al_2O_3/ZSM-5@110 catalyst were 72.5 and 81.4%, respectively (Cai et al., 2016).

Zeolite-based bifunctional catalysts were investigated for the production of DME from CO-rich syngas ($H_2/CO=1$). The catalysts contain a $Cu/ZnO/Al_2O_3$ component for methanol formation and zeolite H-MFI 400 as an acidic component for

dehydration of methanol to DME. The bifunctional catalyst contained 1/1 by weight of $Cu/ZnO/Al_2O_3$ component and H-MFI 400. For all reactions, 2 g of each catalyst with a particle size of 80 to 355 µm was used. The reaction temperature and pressure were 250 ℃ and 51 bar, respectively. The maximum CO conversion and DME selectivity of CZA-Z (composed of 29 wt.% CuO, 18 wt.% ZnO, 18wt.% Al_2O_3 and 35 wt.% SiO_2) catalyst with H-MFI 400 was 48 % and 69%, respectively (Ahmad et al., 2014).

For the direct synthesis of DME from CO hydrogenation over the physical mixture of commercial $CuO/ZnO/Al_2O_3$ (C302, Southwest Research & Design Institute Chemical Industry, China, denoted as CZA) catalyst and the H-form zeolites (HBFZ or HY), CZA/HBFZ has higher activity and stability than CZA/HY. Bifunctional catalysts were prepared by physically mixing CZA and H-form zeolites at a weight ratio of 2:1. Syngas (60.8% H_2, 27.2% CO, 4.8% CO_2, and 3.2% Ar) with a space velocity of 1500 h^{-1} was supplied to the reactor at 5.0 MPa and 250°C. The conversion of CO and the selectivity to DME over CZA/HBFZ are 94.2% and 67.9%, respectively, under 250°C, 5.0 MPa, and 1500 h^{-1} (Yan et al., 2013).

The syngas-to-DME reactions were carried out in a fixed bed stainless steel reactor containing 0.7 g of catalyst. The $Cu\text{-}ZnO\text{-}Al_2O_3$ methanol synthesis catalyst precursor, often known as CZA (nominal Cu:Zn:Al atomic ratio: 6:3:1) and six different zeolites (ZSM-5, FER, IM-5, TNU-9, MCM-22, ITQ-2) were used in this study. The reaction conditions were set at 4.0 MPa and 260 ℃, and the flow rate of the feed gas mixture (90 vol% syngas & 10 vol% Ar) with a molar composition of 66% H_2, 30% CO, 4% CO_2 was adjusted to achieve a space velocity of 1700 $cm^3_{syngas}/(g_{cat}\ h)$. Under these conditions, all catalysts (CZA/zeolite hybrid catalysts) exhibited DME selectivity of 63-65% (García-Trenco et al., 2013).

STA incorporated mesoporous catalyst TRC-75(L), which is synthesized in the laboratory, for methanol dehydration, and a commercial Cu–Zn-based methanol reforming catalyst (HIFUEL-R120-Alfa Aesar) was investigated to produce DME for syngas. The weight ratio of the catalysts for the synthesis and dehydration of

methanol was preserved to one and was called TRC-75(L)-C. 0.2 g of this catalyst was used for the reaction. Activity tests were conducted in the temperature range of 250–400 °C at 50 bar. At temperatures less than 275 °C, DME selectivity values approaching 60% were obtained at 50 bar with 1/1 of the CO/H_2 feed stream (Celik et al., 2013).

Catalytic performances of different alumina-based catalysts to dehydrate methanol to make dimethyl ether were examined in the study of Tokay et al (2012). Alumina impregnated SBA-15 catalyst, a mesoporous aluminosilicate catalyst and the commercial alumina catalyst (Toyo Engineering Co.) were used to dehydrate methanol to DME. The reactor was made of stainless steel and had an internal diameter of 1/4 inch. The reactor's center was filled with the catalyst. An evaporator was initially filled with liquid methanol using a syringe pump. At 150 ℃, the evaporation chamber was maintained. The temperature range used for reaction experiments was 120 to 450 ℃. 0.2 g of catalyst was placed into the reactor. The reactor's input stream had a total flow rate of 44.2 cm^3/min and contained 0.5 moles of methanol. High Brønsted acidity in SBA-15 treated with alumina made it easier to produce dimethyl ether. At temperatures above 300 °C, alumina impregnated SBA-15 catalyst demonstrated close to equilibrium methanol conversion values and approximately 100% DME selectivity. Even at temperatures lower than 300 ℃, the commercial alumina catalyst (Al-T) successfully synthesized DME from methanol (Tokay et al., 2012).

In the study of Ciftci et al (2012), TPA incorporated silica structured mesoporous catalysts (TRC-W40) and MCM-41 catalysts (TPA@MCM-41) were investigated for DME production from methanol and for diethyl ether and ethylene from ethanol. TPA was loaded to MCM-41 using impregnation, and a one-pot hydrothermal synthesis method. Catalysts produced with impregnation and one-pot method were designated as TPA@MCM-41 and TRC-W40, respectively. The TRC-W40 and TPA@MCM-41 catalysts' catalytic abilities were examined during the vapor phase dehydration of ethanol and methanol. 0.2 g fresh catalyst was put into the fixed bed flow reactor. A syringe pump was used to inject liquid methanol into the evaporator

at a flow rate of 2.9 ml/h. Before the reactor, an evaporator was situated and its temperature was maintained at 150 °C. Alcohol was evaporated and helium was combined in the evaporator 1/1. The gas combination was delivered to the reactor at a total flow rate of 44 ml/min. It was discovered that DME yield reached a maximum at around 200 °C in the presence of TPA@MCM-41, which has high Brønsted acidity. TRC-W40 was more stable and showed excellent activity in methanol dehydration, with 100% DME selectivity at temperatures less than 300°C (Ciftci et al., 2012).

The activities of STA incorporated structured silicate catalysts in the production of DME from the methanol dehydration reaction were investigated in a study. In a flow system operating between 180 and 350 °C, methanol dehydration reaction was performed. An evaporator was first supplied with methanol using a syringe pump at a flow rate of 2.1 mL/hr. In the evaporator, it was combined with He gas to change the reactor feed stream's chemical makeup. Methanol's volume proportion in this stream was set to 0.48. By varying the amount of catalyst (0.1-0.3 g) deposited in the tubular reactor, catalytic activity test studies were conducted at various space times (at 0.14, 0.27, and 0.41 $s.g.cm^{-3}$). The catalysts with a W/Si ratio of 0.4 in the synthesis solution (TRC-75(L)) demonstrated extremely high DME selectivity values approaching 100%. With the new STA incorporated mesoporous catalysts, the best operating temperature for methanol dehydration was between 200-250 °C (Ciftci et al., 2010).

2.5 The Aim of This Study

In recent years, finding alternative energy sources to address environmental crises and energy shortage challenges has become one of the main themes. Due to rising energy demand and its ecologically friendly quality in the twenty-first century, DME, manufactured from methanol dehydration or straight from syngas, is generating a lot of interest as a clean alternative fuel. Creating a bifunctional catalyst

that is active and selective for DME product in single-step DME synthesis from syngas is a difficult task that has gained attention recently.

Because of their high proton mobility and good redox properties, heteropolyacids are regarded as one of the literature's most promising solid acid candidates. Main disadvantage of heteropolyacids is its extremely low surface area and almost nonporous structure. Therefore, a support material is required.

Silica aerogels have become quite popular because of their high specific surface area, high porosity, low density, and high thermal insulation value. Thus, mesoporous silica aerogel was deemed suitable support material for synthesizing bifunctional DME catalysts since it has never been used in DME synthesis in the literature before.

Hence, the aim of this study is:

- To synthesize silica aerogel and metal-loaded silica aerogel
- To characterize the physical and chemical properties of the synthesized catalysts using various characterization techniques
- To perform activity test of the synthesized catalysts
- To investigate the effect of STA loaded amount on the DME selectivity
- To determine the most active catalyst among the synthesized catalysts for the direct synthesis of DME from syngas

CHAPTER 3

THERMODYNAMIC ANALYSIS

The single-step DME synthesis from syngas, including CO and H_2, has four main reactions (R1, R2, R3, and R4).

$CO + 2H_2 \rightleftharpoons CH_3OH$ $\quad \Delta H_{298}^0 = -90.4 \frac{kJ}{mol}$ (R1)

$CO_2 + 3H_2 \rightleftharpoons CH_3OH + H_2O$ $\quad \Delta H_{298}^0 = -49.4 \frac{kJ}{mol}$ (R2)

$2CH_3OH \rightleftharpoons CH_3OCH_3 + H_2O$ $\quad \Delta H_{298}^0 = -23.0 \frac{kJ}{mol}$ (R3)

$H_2O + CO \rightleftharpoons H_2 + CO_2$ $\quad \Delta H_{298}^0 = -41.0 \frac{kJ}{mol}$ (R4)

The general stoichiometry of DME synthesis from syngas, including CO and H_2, can be expressed as (R5) and (R6) in direct DME synthesis (Azizi et al., 2014; Bayat & Dogu, 2016; Mondal & Yadav, 2019):

$3CO + 3H_2 \rightleftharpoons CH_3OCH_3 + CO_2$ $\quad \Delta H_{298}^0 = -244.8 \frac{kJ}{mol}$ (R5)

$2CO + 4H_2 \rightleftharpoons CH_3OCH_3 + H_2O$ $\quad \Delta H_{298}^0 = -203.8 \frac{kJ}{mol}$ (R6)

The conventional methanol production system is a two-step process in which methanol formation and methanol dehydration to DME are consecutive reactions. In the DME production, due to highly exothermic reactions, they are notably restricted via the thermodynamic equilibrium. Thus, in the direct DME synthesis, a single-step process, methanol is produced and then consumed to DME in the dehydration process at the same reactor (Azizi et al., 2014; Bayat & Dogu, 2016; Mondal & Yadav, 2019).

Thermodynamic analysis of the reactions in DME synthesis is critical to determining the operating conditions of the reactor. Thermodynamic equilibrium calculations were made using Gaseq software based on the Gibbs Free Energy minimization.

Figure 3.1. shows that the influence of pressure and temperature changes on equilibrium CO conversion for the molar one to one ratio of CO/H_2. When reaction pressure increases, equilibrium CO conversions rise because of reaction stoichiometry. Furthermore, the Le Chatelier principle increases conversion with increasing pressure, shifting the overall reaction to product sides. High pressure is necessary for high equilibrium conversion. According to Figure 3.1., the increase in equilibrium conversion from 40 to 50 bar and 50 to 70 bar is roughly similar at 200-300 °C. For 70 bar, the operating price rises, and the operational risks increase. Therefore, operating pressure was selected as 50 bar in the experiment.

Figure 3.1 demonstrates that a similar CO conversion trend according to temperature is seen at high pressures except for 1 bar. The CO conversion at 250 °C at 50 bar is approximately 6% higher than at 275 °C. The CO conversion at 50 bars 275 °C is 83.2%. Operating temperature was chosen as 275 °C in the experiment.

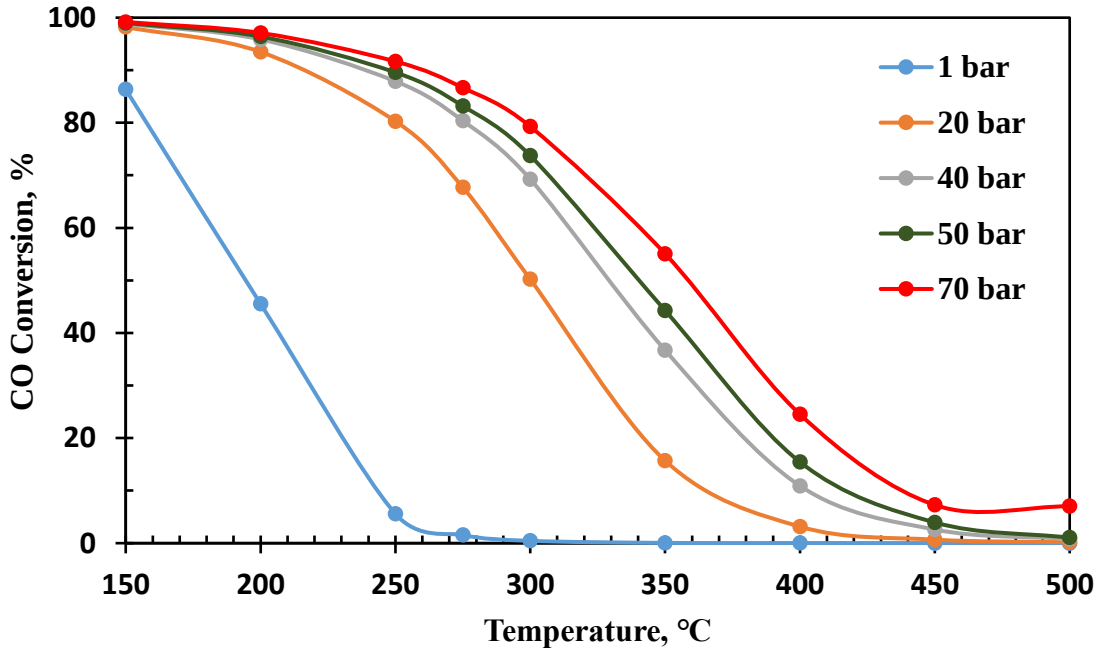

Figure 3.1. Influence of pressure on CO conversion for molar $CO/H_2=1/1$

In addition to pressure and temperature, feed composition is most important. Syngas can be specially produced for different uses according to the required H_2 and CO composition. Among the different synthesis gas production methods, partial catalytic oxidation of methane produces the CO/H_2 ratio required for application in DME synthesis. The increase in H_2 in the feed gas mixture increases the CO conversion. However, the reverse trend is observed for the WGSR because the reaction order is 2 for the methanol synthesis reaction and 1 for the WGSR (Mondal & Yadav, 2019). The influence of feed composition was investigated in Figure 3.2. Figure 3.2 shows that CO conversion is enhanced by increasing CO/H_2 ratio. However, a further CO/H_2 ratio increase does not significantly affect the CO conversion. In terms of CO conversion, a high CO/H_2 ratio is good, but considering the DME mol fraction, the CO/H_2 ratio is 1/1 better as seen in Figure 3.3.

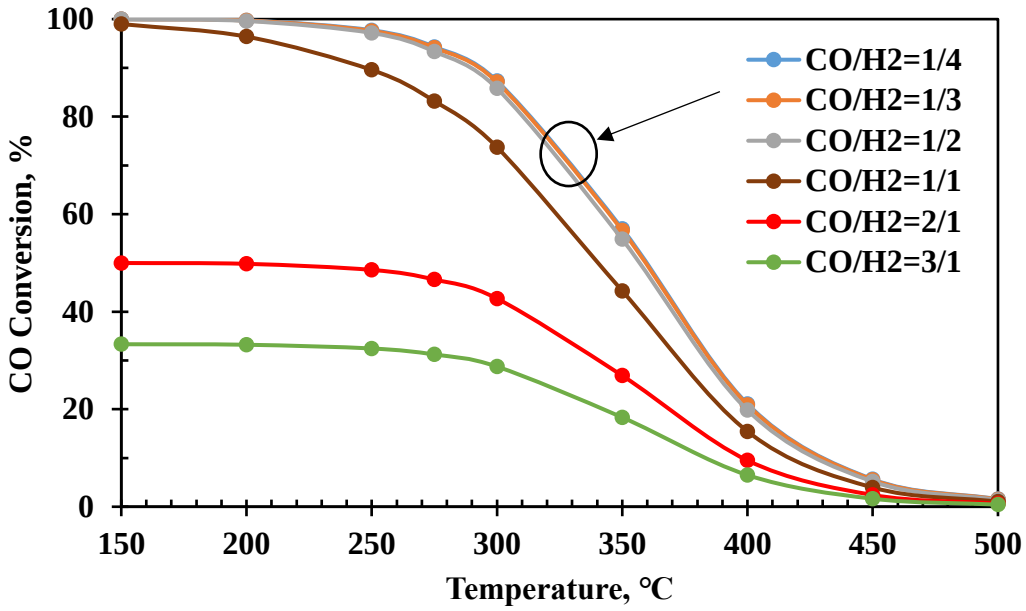

Figure 3.2. Influence of molar CO/H_2 feed ratio on CO conversion at 50 bar

Figure 3.3 shows that the CO/H_2 feed ratio of 1/1 gives a higher DME mole fraction and CO conversion at 50 bar and between 200-275 ℃ according to thermodynamic analysis. As a result, the operating CO/H_2 feed ratio was selected as 1/1. This result is compatible with the literature. According to Azizi et al., optimum H_2/CO is 1/1 for the optimum syngas conversion. Due to all exothermic reactions in the DME

synthesis, DME synthesis is preferred at lower temperatures because by-products and coke are formed at higher temperatures (Azizi et al., 2014).

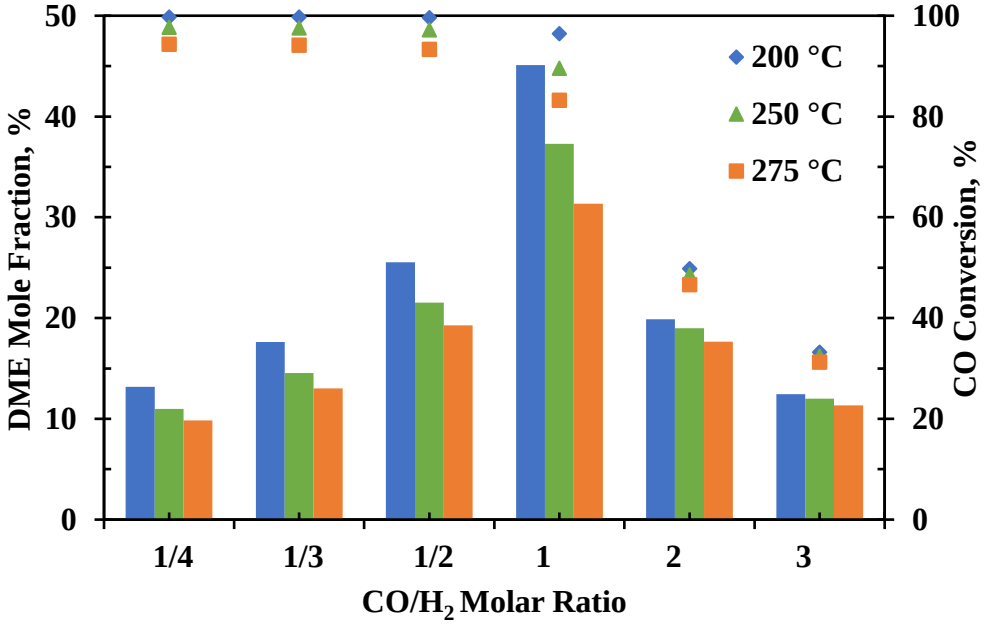

Figure 3.3. Influence of molar CO/H_2 ratio on DME mole fraction and CO conversion at 50 bar and temperature range of 200-275 °C (Bars: DME mole fraction; Symbols: CO conversion)

The highest DME mole fraction is obtained at 200 °C. Since earlier studies were at 275°C the temperature was chosen as 275°C to compare with the literature results. In other words, temperature, pressure, and feed composition (CO/H_2) were selected as 50 bar, 275 °C, and 1/1, respectively, to produce DME more economically and with higher DME selectivity. The aim of this experiment is to obtain high CO conversion and DME selectivity by loading metal onto the silica aerogel support material at the conditions selected above.

CHAPTER 4

EXPERIMENTAL

The experimental section of this study comprises three parts: synthesis and characterization of the catalysts and catalyst activity test for producing DME, which is carried out in the Chemical Reaction Engineering Laboratory at METU.

4.1 Synthesis of Catalysts

The synthesis of the catalysts can be separated into two parts: synthesis of the support material and metal loading to the support. Silica aerogel, the support material, was synthesized. The impregnation method was utilized for the metal loading to the support.

4.1.1 Synthesis of Silica Aerogel

In the silica aerogel synthesis, 5.64 g ethanol (Sigma Aldrich), 10.01 g tetraethylorthosilicate (TEOS, Merck), and 62 µL of 1M hydrochloric acid (HCL, 37 v/v%, Merck) were added to 1.73 g distilled water, respectively, at room temperature. Then, the prepared solution was mixed on a magnetic stirrer at room temperature for 2 hours in an airtight beaker. 3.85 g distilled water and 9.92 g ethanol were added to the prepared solution. Later, 650 µL of 1M ammonia (NH_3, 25 v/v%, Merck) solution and 800 µL of 1M ammonium fluoride (NH_4F, Merck) solution are added dropwise by stirring the solution. After adding enough ethanol to cover the gel completely, it is kept closed at room temperature for eight hours. Ethanol was changed with hexane (Sigma Aldrich), and then the gel was put into a water bath of 45°C (Sivri et al., 2019). In order to slow down the reaction rate during the surface modification process, n-Hexane solvent was also utilized to dilute the concentrations

of the silylating reagents (Wu et al., 2011). After two hours, hexane was replaced with hexane. Then, trimethylchlorosilane (TMCS, Merck) was added to the solution. At that time, water and HCl vapor were observed. The new hexane was added to the gel as much as the water volume in the solution. After, the gel-hexane mixture was put into a water bath of 45 ℃ for 5 hours. After 5 hours, hexane in the gel-hexane mixture was changed with a new one and then put into a water bath of 45 ℃ for another 5 hours. Finally, the hexane in the gel-hexane mixture was filtered, and then the gel was left in an oven at 125 °C for 2 hours (Sivri et al., 2019). All silica aerogels were synthesized at different times. The sample was named SA (silica aerogel). The silica aerogel was calcined at 500 ℃ under a dry air atmosphere for 12 hours. The furnace was heated to 500 ℃ from ambient temperature with a heating rate of 1 ℃/min and remained at 500 ℃ for 12 hours. After the calcination, the sample was named CSA (calcined silica aerogel).

4.1.2 STA or TPA Loading to the Silica Aerogel Support

A certain amount of silicotungstic acid (STA, Sigma Aldrich) or tungstophosphoric acid (TPA, Acros Organics) was dissolved in 10 ml ethanol at room temperature, whereas one gram of SA support was dissolved in 20 ml ethanol at room temperature. After 2 hours, the STA solution was added dropwise to the support solution. Then, the prepared solution was stirred at room temperature for 24 h, and after stirring, the solution was dried at 60 ℃ for 24 h. Finally, the solid catalyst was calcined in a quartz tubular reactor at 375 ℃ under a dry air atmosphere for 6 hours. The reactor was heated to 375 ℃ from ambient temperature with a heating rate of 1 ℃/min and remained at 375 ℃ for 6 hours.

4.1.3 Alumina and STA Impregnation to the Silica Aerogel Support

While one gram of silica aerogel was added to 20 ml of ethanol, 1.39 gram of aluminum nitrate nonahydrate (Merck) was added to 10 ml of ethanol. The well-

mixed aluminum nitrate nonahydrate solution was added dropwise to the well-mixed support solution. Then, the prepared solution was stirred at room temperature for 24 h, and after stirring, the solution was dried at 65 ℃ for eight hours. The Al loaded silica aerogel catalyst was calcined at 500 ℃ under a dry air atmosphere for 12 h. After the calcination, 0.347 g of STA was loaded to silica aerogel-alumina catalyst with similar synthesis steps described in Section 4.1.2. Finally, the solid catalyst was calcined at 375 ℃ under a dry air atmosphere for 6 hours.

4.1.4 The Naming of the Catalyst

The metal-loaded silica aerogels were synthesized using the wet impregnation method. They were named in the SA-XY-ZT format in which SA stands for silica aerogel, X and Z remark the metal percentage in weight, and Y and T are the type of metal loaded. There is no ZT term in a single metal-loaded catalyst. CSA stands for calcined silica aerogel.

A commercial methanol synthesis catalyst was named MSC (Alfa Aesar) for the methanol synthesis reaction. MSC includes 35 wt % of Cu and 20.7 wt.% of Zn. Since copper-based catalysts are widely used in methanol formation reactions, copper-based methanol synthesis catalyst was preferred. A commercial γ-alumina catalyst was named CA (Toyo Engineering Co.) for methanol dehydration catalysts. Alumina is the most often used solid acid catalysts for methanol dehydration because they are stable at high temperatures and pressures, have a large surface area, are inexpensive, and have the majority of acid sites with lower acidities (Mondal & Yadav, 2019). Therefore, a commercial γ-alumina was used as solid acid catalyst.

For example, 10 wt.% STA impregnated silica aerogel was named SA-10STA. Table 4.1 shows all the catalysts synthesized and utilized in the production of DME from syngas.

Table 4.1 List of catalysts utilized in the DME synthesis

Catalyst	Content (wt. %)				
	STA	**TPA**	**Al**	**Cu**	**Zn**
SA-10STA	10	-	-	-	-
SA-24STA	24	-	-	-	-
CSA-24STA	24	-	-	-	-
SA-35STA	35	-	-	-	-
SA-10Al-25STA	25	-	10	-	-
SA-25TPA	-	25	-	-	-
MSC	-	-	-	35	20.7
CA			~100		

4.2 Characterization Techniques of Synthesized Catalysts

Nitrogen physisorption technique, X-ray Diffractometer (XRD), Thermogravimetric analyzer (TGA), Fourier Transform Infrared Spectroscopy (FTIR) and Diffuse Reflectance Infrared Transform Spectroscopy (DRIFTS) were used to characterize the synthesized material.

4.2.1 Nitrogen Physisorption Analysis

The nitrogen physisorption technique is extensively utilized to find the surface area of materials (Thommes & Cychosz, 2014). To determine the surface area, pore-volume, adsorption/desorption isotherms, and pore size distribution, the Micromeritics Tristar II 3020 device at METU Department of Chemical Engineering was used. All samples were degassed at 130 ℃ and 3 hours under vacuum before the analysis. The relative pressure range (P/P_0) was from 0.0001 to 0.99.

4.2.2 X-Ray Diffraction Analysis

XRD analysis is used to examine the crystal structure of materials. Rigaku Ultima-IV diffractometer device in METU Central Laboratory was used, operating at 40 kV and 30 mA. Bragg angle values were adjusted in the range of 10˚-90˚ with a scanning rate of 1˚/min to get XRD patterns.

4.2.3 Thermogravimetric Analysis

TGA is a thermal analysis method where a sample's mass is measured with the temperature changes under air or inert gases such as helium and nitrogen. TGA was used to obtain information about the thermal stability of the catalyst. TGA analysis was performed using Shimadzu DTG-60H device at METU Department of Chemical Engineering under an air atmosphere with a 50 ml/min flow rate and a heating rate of 10°C/min in the temperature range of 25°C-900°C.

4.2.4 Fourier Transform Infrared Spectroscopy (FTIR) Analysis

The FTIR Spectroscopy analysis revealed the bond types of the materials. Materials were analyzed using Perkin Elmer Spectrum One equipment. These samples' FTIR spectra were obtained with a resolution of 4 cm^{-1} and a wavenumber range of 500-4000 cm^{-1}.

4.2.5 Diffuse Reflectance Infrared Fourier Transform Spectroscopy Analysis

DRIFTS analysis of catalysts adsorbed by pyridine was performed using the Perkin Elmer Spectrum One FTIR Spectrometer device. Before analysis, all catalysts were dried at 110 °C and put in a pyridine desiccator for one week. In addition, fresh catalysts dried at 110 °C and pyridine adsorbed catalysts were analyzed between

450–4000 cm^{-1} region via 100 scans at 4 cm^{-1} resolution using a mirror velocity of 0.2 cm/s. The differences between fresh and pyridine adsorption spectra of catalyst were utilized to specify the Lewis or Brønsted acid sites of the catalysts.

4.3 Activity Tests in DME Production System

4.3.1 The DME Reaction System

A high-pressure lab-scale DME production system shown in Figure 4.1 was installed to test activity of the synthesized catalysts. 1/4 inch 316 stainless steel pipes, valves, and fittings were utilized. The tubular reactor is also 1/4 inch and 316 stainless steel. Three mass flow controllers (OMEGA Engineering Inc.) were used to control and set the H_2, CO, and CO_2 gas flowrates. Three pressure gauges were placed before the MFC to measure the inlet pressure of each gas line. To measure the system pressure, a gauge pressure (PAKKENS) was placed at the MFC junction outlet.

At the start of the operation, two additional lines were built to bypass line in the MFCs part and in the reactor part. A reactor bypass system prevents the catalyst slipping from its bed with a sudden pressure change while pressurizing the system. It is also used to relieve the pressure in the system after the reaction time is complete. Check valves with 1/3 psi crack pressure were placed after each MFC and MFC bypass line to prevent backflow when a line had a pressure lower than the downstream pressure.

Reaction pressure was adjusted with a needle valve. The soap bubble meter is used to check the total flowrate of gas mixture in the exit of the reactor.

Heating bands used in the inlet and outlet lines of the reactor are used to prevent the reactants from entering the reactor cold and to prevent condensation of the products. A tubular furnace was used to heat the tubular reactor to reach and maintain the reaction temperature.

The reactor effluent stream was analyzed continuously via Gas Chromatography (GC, Varian CP3800) with Porapak Q packed column and thermal conductivity detector (TCD). Argon was chosen as the carrier gas in GC.

4.3.2 Experimental Procedure

The methanol synthesis catalyst and the methanol dehydration catalyst were physically mixed at a weight ratio of 1:1, and 0.3 g of the catalyst was placed in the middle of the reactor and fixed with glass wool at both ends. Then the reactor was placed in the tubular furnace. The reactor temperature was increased to 275 ℃ with a heating rate of 10 ℃/min. When the temperature reaches 275 C, hydrogen gas is fed to the reactor with a flow rate of 12.5 ml/min and catalyst was reduced for 30 minutes under hydrogen at ambient pressure. At the same time, the entire and exit lines were heated to 150 and 100 °C, respectively, with heating tapes. After the reduction, the hydrogen mass flow controller was closed. In order for the reaction not to start, the furnace temperature is lowered to 130 °C. When the temperature reaches 130 °C, the system was pressurized with the desired gas composition via bypass lines. The valves in the bypass lines were turned off when the system reached 50 bar. The reactor pressure was then monitored on the pressure gauge for 5 minutes while the outlet line of the reactor was turned off for the leaking test. Gas flow rates were adjusted with MFCs, and the outlet flow rate of the reactor exit was measured using a soap bubble meter.

In each catalytic performance test, the reaction time was 5 hours. The effluent of the reactor was analyzed via GC at 50-minute intervals during activity testing. After 5 hours, the reactor was allowed to cool, the gases fed to the reactor were turned off, and the system pressure was relieved from the bypass lines. The heat band temperatures at the reactor inlet and outlet were left at 200 ℃ until the reactor cooled down to avoid condensation along the reactor line.

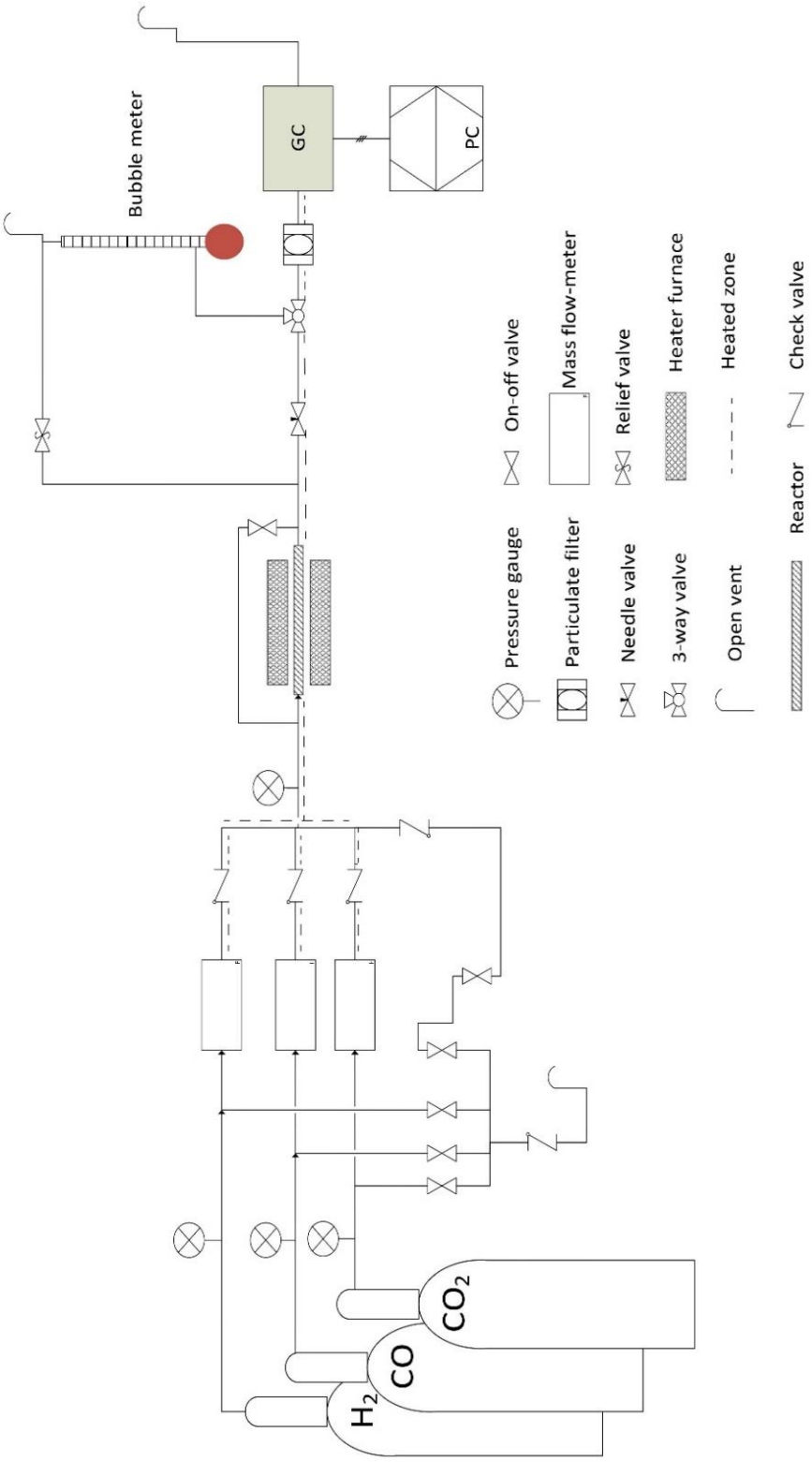

Figure 4.1. DME production system

Repeatability experiments were carried out using MSC and CA together three times. The GC analysis condition and column temperature detail are given in Tables 4.2 and 4.3.

Table 4.2 GC analysis condition

	Temperature (°C)	**Pressure (psi)**	**Flowrate (ml/min)**	**Carrier gas**
TCD	200	-	30	Ar
Column	38-170	5	-	Ar

Table 4.3 GC column temperature program

Temperature (°C)	**Hold duration (min)**	**Heating rate (°C/min)**
38	6	-
120	1	4
130	0.1	1
170	0.4	20

CHAPTER 5

RESULTS AND DISCUSSION

In this chapter, the catalysts' characterization and activity test results are given and discussed. All catalysts used in this study were characterized via different techniques to understand the influence of material properties on catalytic activity.

5.1 Characterization Results of The Catalysts

MSC was utilized as metallic catalyst to produce methanol from syngas. STA, TPA, and alumina were also impregnated into silica aerogel which was used as support material, and the synthesized catalysts were used for dehydration of methanol to DME. Commercial alumina (CA) was also used for dehydration of methanol to DME. Nitrogen physisorption, XRD, TGA, FTIR, and DRIFTS were used to characterize the synthesized catalysts to investigate the surface area and porosity, crystal structure, and acidity of the catalysts.

5.1.1 Nitrogen Physisorption Analysis

Nitrogen physisorption of commercial methanol synthesis catalyst (MSC), silica aerogel support, and metal-loaded silica aerogels was examined in this part.

5.1.1.1 Methanol Synthesis Catalyst

A commercial methanol synthesis catalyst was used as a metallic catalyst to produce methanol during the direct method production of DME from syngas. Figure 5.1 shows the nitrogen adsorption/desorption isotherm of MSC. MSC displayed a characteristic mesoporous Type IV isotherm with a hysteresis beginning from about

P/P_0 value of 0.65 according to IUPAC classification. The MSC isotherm exhibited any limiting adsorption at high P/P_0 and can be classified as an H2 type hysteresis showing disordered pores. Because of the low N_2 adsorbed volume, a low surface area was expected. There are also micropores in MSC. H2 type hysteresis indicates that MSC is a non-uniform material, it has an uneven pore distribution, and has a wide pore distribution.

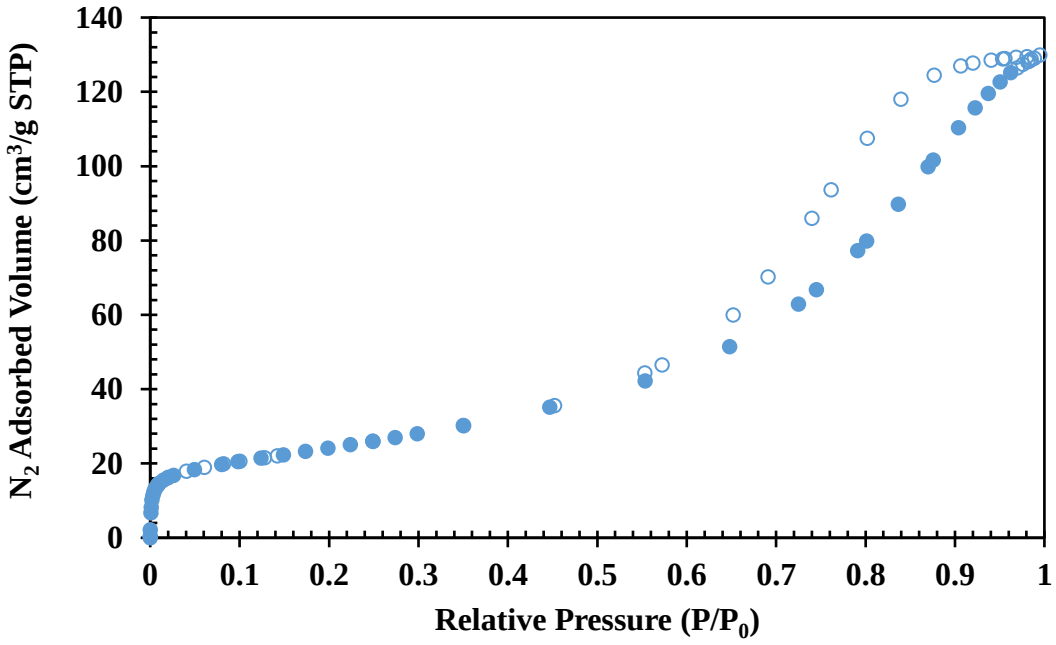

Figure 5.1. Nitrogen adsorption/desorption isotherms of commercial MSC (Filled symbol: adsorption branch, empty symbol: desorption branch)

Figure 5.2 shows BJH desorption pore size distribution, and Table 5.1 demonstrates the physical properties of MSC. The average pore size of MSC is 7 nm. Pore size distribution of MSC indicates mesoporous structure range and MSC has a large pore diameter between 2-50 nm, which shows that it is compatible with the nitrogen adsorption/desorption isotherm.

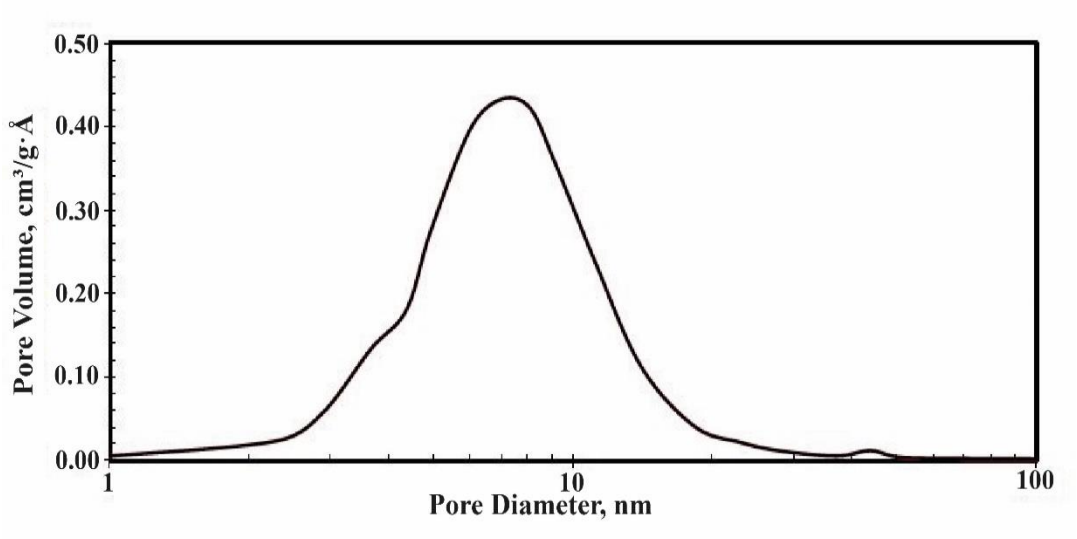

Figure 5.2. Pore size distribution of commercial MSC

The surface area of MSC is 87 m^2/g. The low surface area is compatible with the low N_2 adsorbed volume in the nitrogen adsorption/desorption isotherm. The microporosity of the MSC catalyst was 13.3%.

Table 5.1 The physical properties of commercial MSC catalyst

Catalyst	Multipoint BET Surface Area (m^2/g)	BJH Desorption Pore Volume (cm^3/g)	BJH Desorption Average Pore Diameter (nm)	Micro-porosity (%)
MSC	87	0.20	7.0	13.3

5.1.1.2 Silica Aerogels and Metal Loaded Silica Aerogels

Nitrogen adsorption/desorption isotherms and pore size distribution of pure silica aerogels synthesized at different times are given in Figures 5.3 and 5.4.

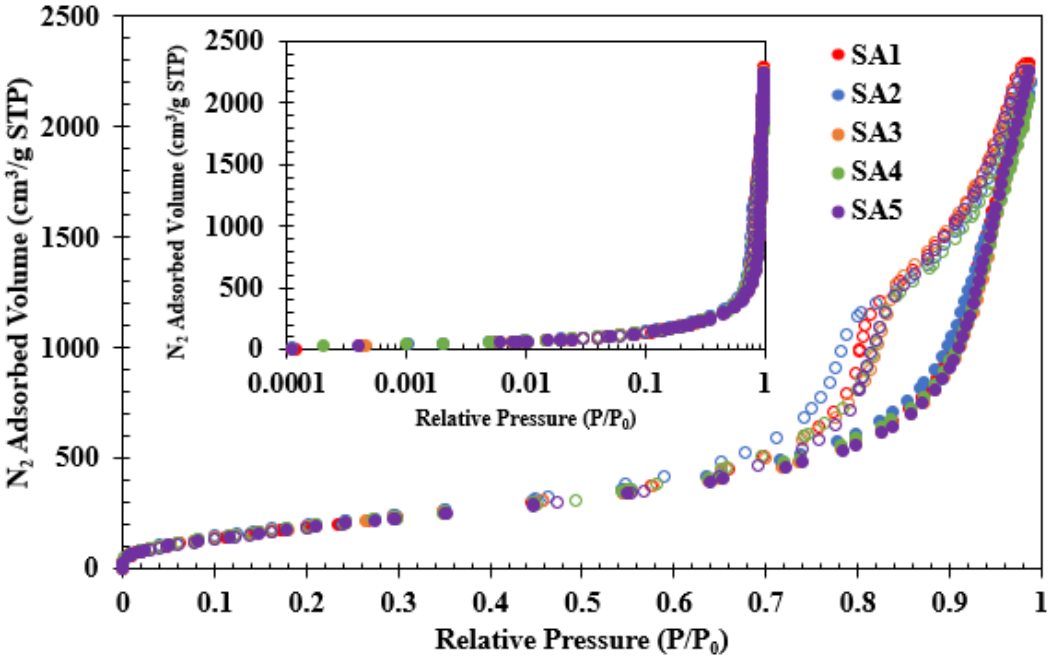

Figure 5.3. N_2 adsorption/desorption isotherms of pure SA (Filled symbol: adsorption branch, empty symbol: desorption branch)

In Figure 5.3, N_2 adsorption/desorption isotherms of pure silica aerogels synthesized at different times showed Type IV isotherms with H3 type hysteresis loop, indicating the presence of nonuniform, slit-shaped pores and mesoporous materials. According to Figure 5.4, silica aerogels include mainly mesopores. However, there are also macropores and micropores. Silica aerogels are in the same pore size range with little variation except for SA2. This is compatible with N_2 adsorption/desorption isotherm of SA2.

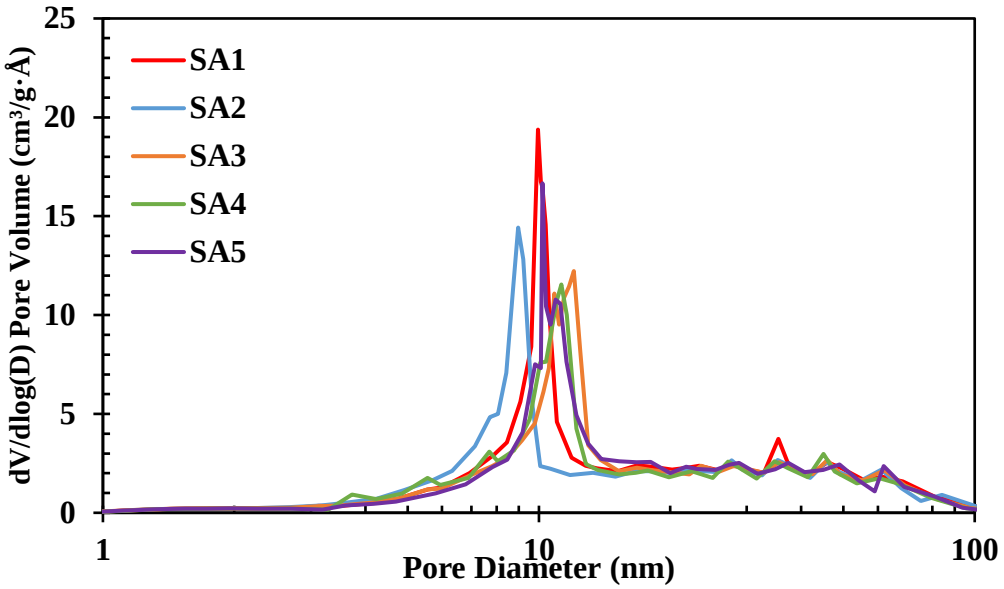

Figure 5.4. Pore size distribution of pure SA materials

The physical properties of pure silica aerogels synthesized at different times are given in Table 5.2. The multipoint BET surface area of pure silica aerogels varies between 778 and 816 m^2/g. The average pore size and pore volume of them vary between 10.1 and 114 nm, and between 3.24 and 3.54 cm^3/g, respectively. The average multipoint BET surface area of silica aerogels produced at different times is 793 m^2/g, their pore volume is 3.44 cm^3/g, and the pore diameter is 10.9 nm. As seen from these results, the synthesis method of silica aerogel is reliable and reproducible.

Table 5.2 The physical properties of pure silica aerogels

Catalyst Support	Multipoint BET Surface Area (m^2/g)	BJH Desorption Pore Volume (cm^3/g)	BJH Desorption Average Pore Diameter (nm)	Micro-porosity (%)
SA1	785	3.54	11.0	4.67
SA2	816	3.41	10.1	4.96
SA3	783	3.50	11.1	5.17
SA4	802	3.29	10.7	5.26
SA5	778	3.48	11.4	4.77
Average	793±14.1	3.44±0.09	10.9±0.4	4.96±0.23

According to Figure 5.5, while the type of hysteresis changed for calcined SA, the type of isotherms of SA and CSA was unchanged. The pure SA and CSA indicated Type IV isotherm. Whereas the pure SA showed H3 type hysteresis loop with a hysteresis beginning from about 0.7 P/P_0, CSA indicated an H1 type hysteresis loop with a hysteresis beginning from about 0.8 P/P_0 due to a change in pore structure in SA as a consequence of removing methyl group ($-CH_3$) in the silica aerogel structure during the calcination. The hysteresis of CSA is shifted to the left relative to SA, indicating that the CSA average pore diameter is larger.

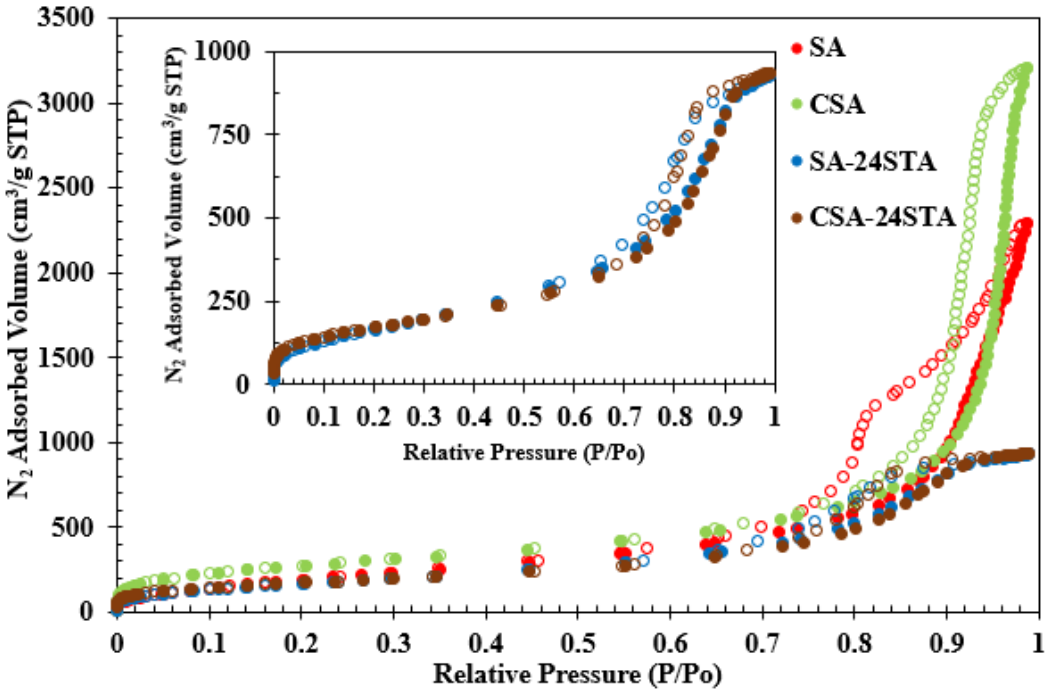

Figure 5.5. N_2 adsorption/desorption isotherms of pure and calcined SA, SA-24STA, and CSA-24STA (Filled symbol: adsorption branch, empty symbol: desorption branch)

According to Figure 5.6, the pore diameter distribution of calcined silica aerogel shifts to higher pore diameters than uncalcined silica aerogel. This is compatible with the isotherm. The calcination process increases the pore diameter of silica aerogel with the removal of $-CH_3$ groups which are formed by modification of silica aerogel with TMCS. According to Table 5.3, the pore diameter of SA and CSA is 10.9 and 13.2 nm, respectively.

According to Figure 5.5, STA loading into SA and CSA led to a decrease in the adsorbed volume of N_2 because of metal loading. Furthermore, STA loading altered the pore structure because the H3 type hysteresis loop of SA changed to the H1 type hysteresis loop, which expresses a narrower pore size distribution and implies that the material had a mesoporous structure. Nonetheless, the Type IV isotherms remained unchanged for the SA-24STA and CSA-24STA catalysts in Figure 5.5.

According to Figure 5.6, STA loaded into SA and CSA caused the macropores to vanish. There were only mesopores because STA accommodates into the pores of the silica aerogel. Settlement of STA in the pores resulted not only in a decrease in the pore size of the macropores but also in clogging of the pores. Consequently, this resulted in a decrease in the average pore diameter.

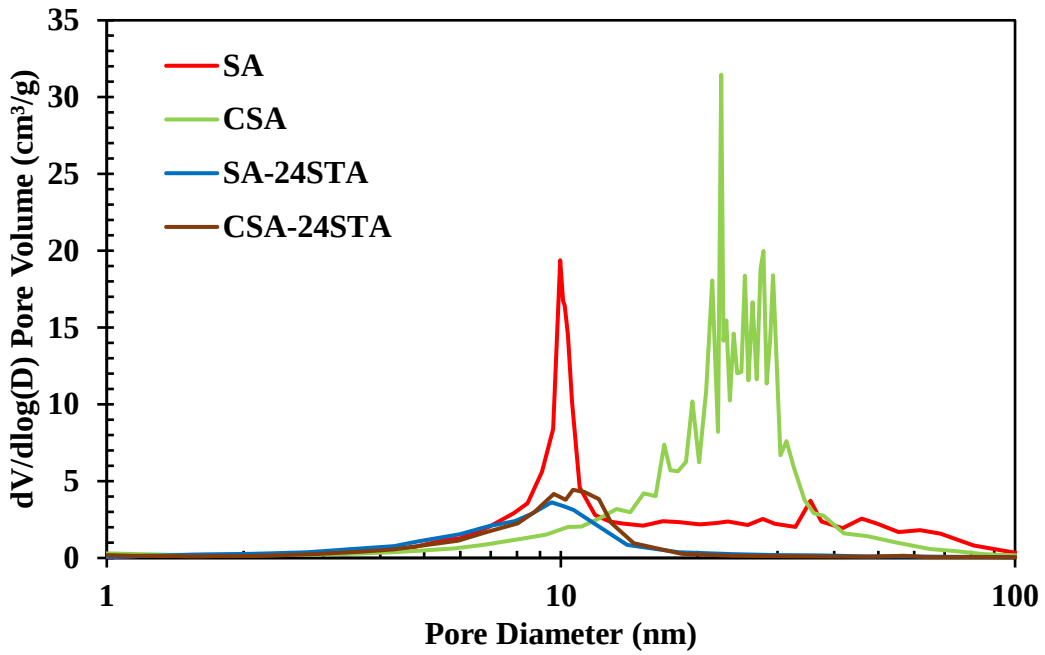

Figure 5.6. Pore size distribution of pure and calcined SA, SA-24STA and CSA-24STA

The physical properties of SA, CSA and STA loaded into them are given in Table 5.3. SA-24STA and CSA-24STA had BET surface area of 629 and 615 m^2/g, respectively. BJH desorption average pore diameters of SA-24STA and CSA-24STA were 6.19 and 6.41 nm, respectively. The decrease in pore diameter and pore volume indicates that STA clogs the pores.

Table 5.3 The physical properties of pure and calcined SA, SA-24STA and CSA-24STA

Catalyst	Multipoint BET Surface Area (m^2/g)	BJH Desorption Pore Volume (cm^3/g)	BJH Desorption Average Pore Diameter (nm)	Micro-porosity (%)
SA	793±14.1	3.44±0.09	10.9±0.4	4.96±0.23
CSA	975	4.97	13.2	9.13
SA-24STA	629	1.44	6.19	9.46
CSA-24STA	615	1.46	6.41	11.1

N_2 adsorption/desorption isotherms and pore size distributions of 10%, 24%, and 35% by weight of STA loaded SA, and 10% Al and 25% STA by weight loaded SA were demonstrated in Figures 5.7-5.8.

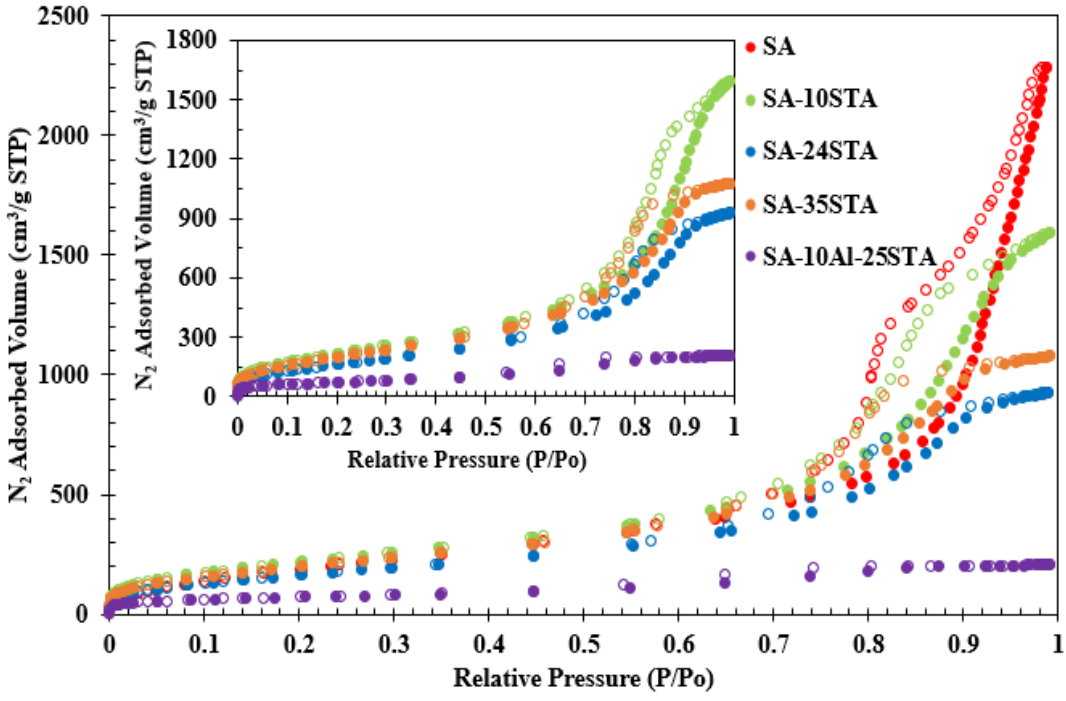

Figure 5.7. N_2 adsorption/desorption isotherms of pure and metal-loaded silica aerogel catalysts (Filled symbol: adsorption branch, empty symbol: desorption branch)

According to Figure 5.7, pure silica aerogel exhibited type IV isotherm with H3 type hysteresis loop with a hysteresis beginning from about 0.7 P/P_0. However, an increase in metal amount gave rise to diminish N_2 adsorbed volume. STA loading into SA changed the pore structure, being concluded an alteration in hysteresis loop from H3 to H1 with a hysteresis starting from about 0.74, 0.71, 0.72 and 0.54 P/P_0 of SA-10STA, SA-24STA, SA-35STA, and SA-10Al-25STA, respectively. Except for SA-10Al-25STA, the hysteresis is shifted to the right. This shows that the average pore diameter is the highest in SA-10STA and the lowest pore diameter in SA-10Al-25STA. However, the different amounts of metal loaded into SA did not change the type IV isotherms. H1 type hysteresis loop shows a narrower pore size distribution. Co-loading of aluminum and STA in SA caused less N_2 adsorbed volume than that of others.

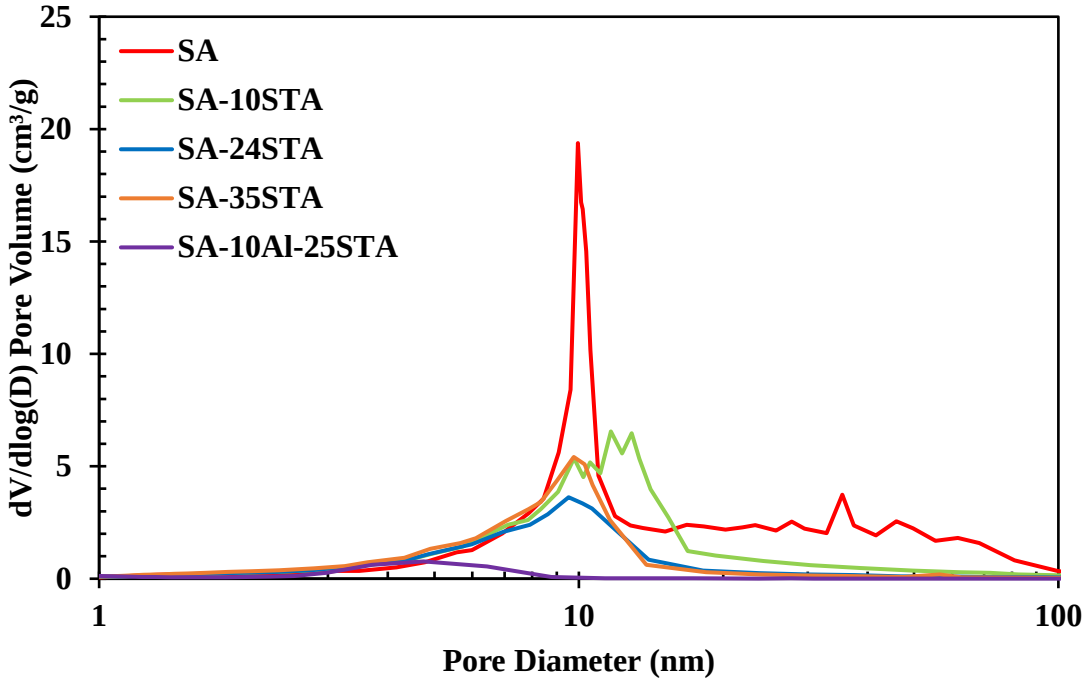

Figure 5.8. Pore size distribution of pure and metal-loaded silica aerogel catalysts

According to Figure 5.8, mesopores and macropores are found in silica aerogel. However, when STA was loaded onto the silica aerogel, macropores are clogged with loaded metals, leaving only mesopores because STA accommodates the silica aerogel pores, resulting in a reduction in the pore size of the macropores but also

pore clogging. Co-loading of aluminum and STA resulted in a lower pore diameter. As seen in Figure 5.8, the highest average pore diameter in the pore distribution was obtained with SA-10STA and the lowest pore diameter was obtained with SA-10Al-25STA. It is seen that the pore diameter distribution with metal loading is narrower than that of pure SA, and these results are consistent with the isotherm.

The physical properties of SA, STA loaded into SA, and Al and STA loaded into SA are given in Table 5.4. SA-10STA and SA-24STA had BET surface areas of 828 and 629 m^2/g, respectively. BJH desorption average pore diameters of SA-10STA and SA-24STA were 8.04 and 6.19 nm, respectively. SA-35STA and SA-10Al-25STA also had BET surface areas of 523 and 248 m^2/g, respectively. BJH desorption average pore diameters of SA-35STA and SA-10Al-25STA were 5.50 and 3.59 nm, respectively. Except for SA-10STA, a decrease in surface area and pore volume values was observed with metal loading.

Table 5.4 The physical properties of SA, SA-10STA, SA-24STA, SA-35STA, and SA-10Al-25STA

Catalyst	Multipoint BET Surface Area (m^2/g)	BJH Desorption Pore Volume (cm^3/g)	BJH Desorption Average Pore Diameter (nm)	Micro-porosity (%)
SA	793±14.1	3.44±0.09	10.9±0.4	4.96±0.23
SA-10STA	828	2.47	8.04	7.67
SA-24STA	629	1.44	6.19	9.46
SA-35STA	523	1.06	5.50	9.91
SA-10Al-25STA	248	0.33	3.59	23.0

Furthermore, because STA particles are located in the mesopores and macropores of silica aerogel, increasing the STA amount decreases the BET surface area, pore

diameter, and pore volume of the catalysts, which may increase microporosity. Co-loading of aluminum and STA resulted in more microporosity.

N_2 adsorption/desorption isotherms and pore size distributions of SA, SA-24STA, and SA-25TPA were depicted in Figures 5.9-5.10.

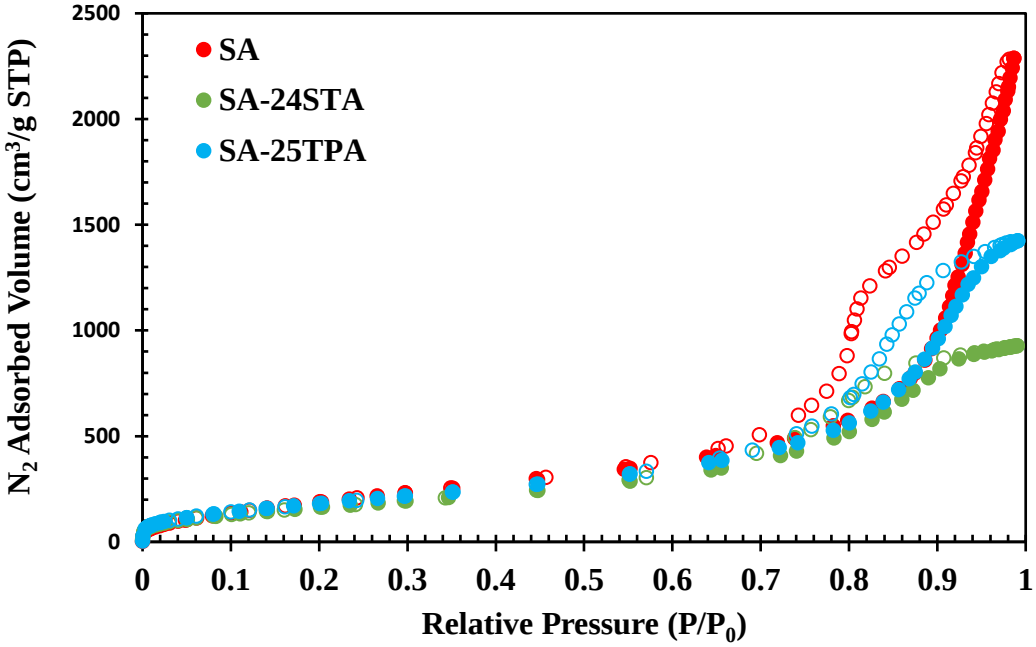

Figure 5.9. N_2 adsorption/desorption isotherms of pure SA, SA-24STA, and SA-25TPA (Filled symbol: adsorption branch, empty symbol: desorption branch)

According to Figure 5.9, STA and TPA loading into SA changed the pore structure, being concluded an alteration in the hysteresis loop from H3 to H1 with a hysteresis starting from about 0.71 of SA-24STA and 0.74 P/P_0 of SA-25TPA. H1 type hysteresis loop shows a narrower pore size distribution. 25% by weight of TPA loaded SA had more N_2 adsorbed volume than one of 24% by weight of STA loaded SA.

According to Figure 5.10, silica aerogel contains mesopores and macropores. Nevertheless, when STA and TPA were loaded onto the silica aerogel, the macropores vanished, leaving only mesopores since STA and TPA accommodate the

silica aerogel pores. As a result, macropore size decreases, and the pore is clogged. The pore distribution is compatible with the isotherm.

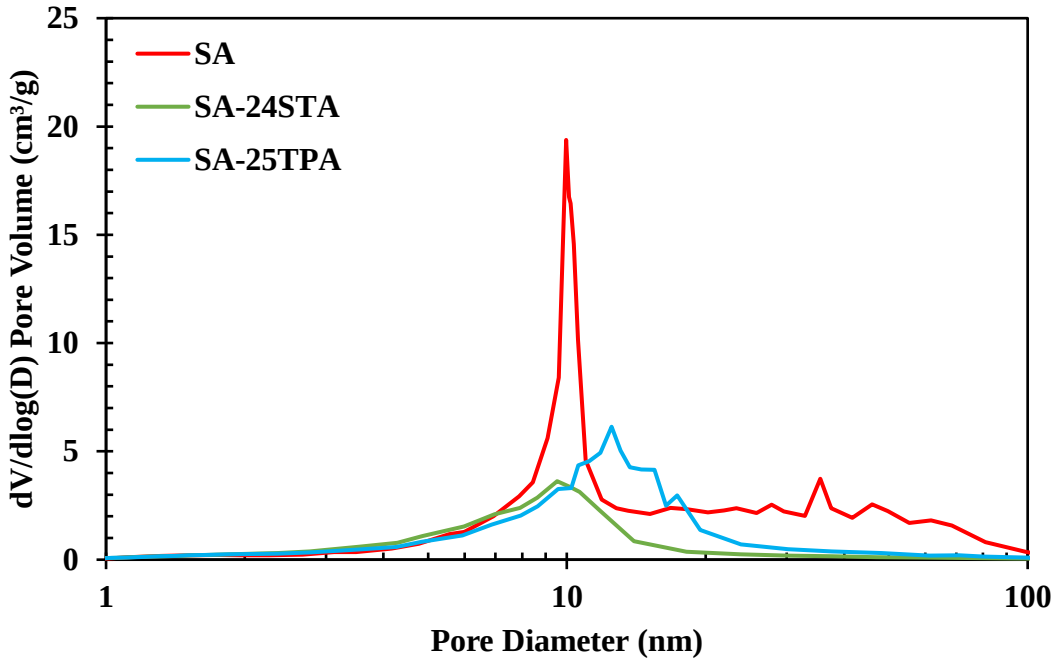

Figure 5.10. Pore size distribution of SA, SA-24STA, and SA-25TPA

The physical properties of SA, STA and TPA loaded into SA are given in Table 5.5. SA-24STA and SA-25TPA had BET surface areas of 629 and 709 m^2/g, respectively. BJH desorption average pore diameters of SA-24STA and SA-25TPA were 6.19 and 8.41 nm, respectively. BJH desorption pore volume of SA-24STA and SA-25TPA were 1.44 and 2.21 cm^3/g, respectively. TPA loaded SA had less microporosity than STA loaded SA.

Table 5.5 The physical properties of SA, SA-24STA, and SA-25TPA

Catalyst	Multipoint BET Surface Area (m^2/g)	BJH Desorption Pore Volume (cm^3/g)	BJH Desorption Average Pore Diameter (nm)	Micro-porosity (%)
SA	793±14.1	3.44±0.09	10.9±0.4	4.96±0.23
SA-24STA	629	1.44	6.19	9.46
SA-25TPA	709	2.21	8.41	7.07

5.1.2 XRD Analysis

In this part, XRD analysis of STA and TPA loaded silica aerogels and co-loading of aluminum and STA were examined. According to the XRD data, the phases of catalysts were identified using PDF Cards of the metal and/or metal oxide and/or bimetallic forms given in Appendix A.

5.1.2.1 Methanol Synthesis Catalyst

A catalyst capable of producing methanol is primarily required during the single-step production of DME from syngas. A commercial methanol synthesis catalyst was also used as a catalyst for this purpose. The methanol synthesis catalyst underwent XRD analysis to determine its content and crystal structure.

Figure 5.11 shows XRD pattern of the commercial MSC. MSC showed five peaks at 2θ values of 32.2°, 35.9°, 39.3°, 48°, and 67°.

In the XRD pattern of MSC, 2θ value of 31.8˚ was assigned to ZnO (1 0 0). The broad peak between 34.0˚-36.5˚ was assigned ZnO (0 0 2) and ZnO (1 0 1). ZnO (1 0 2) was assigned a peak at 2θ value of 48˚. The broad peak between 35.5˚-36.5˚ was assigned to CuO (-1 1 1) and CuO (0 0 2). CuO (1 1 1) and CuO (2 0 0) were responsible for the peak at 2θ value of 39˚. CuO (-2 0 2) were also assigned a peak at 2θ value of 48˚. The broad peak between 34.0˚-36.5˚ was assigned Cu_2O (111). ZnO (1 0 2) and CuO (-2 0 2) were assigned a peak at 2θ value of 48˚. Due to the overlapping of CuO, ZnO, and Cu_2O in the XRD pattern, broaden peaks with high intensities were observed between 2θ values of 30˚-40˚. According to the XRD analysis, the main peak of metallic Cu (1 1 1), with a 2θ value of 43.3˚, was not observed in the XRD pattern of MSC because MSC was not reduced.

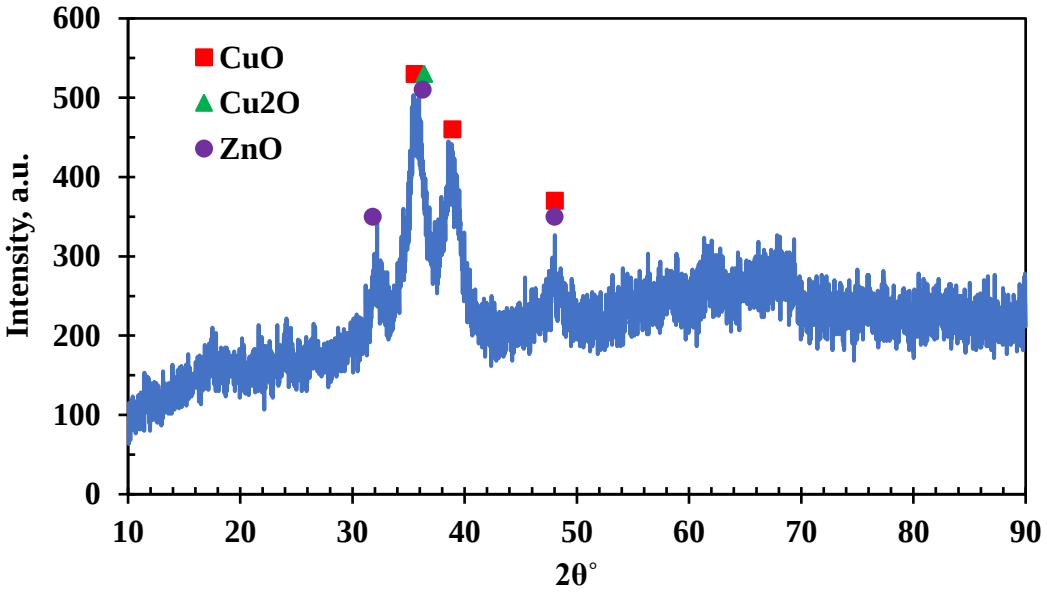

Figure 5.11. XRD pattern of the commercial MSC catalyst

5.1.2.2 Metal Loaded Silica Aerogel

Figures 5.12 and 5.13 show XRD patterns of pure STA and TPA, respectively. In the XRD pattern of STA, 2θ value of 18.06, 20.86, 26.5 28.1, 28.78, 31.06, 32.6, 35.34, 36.94, 45.96, and 53.48 was assigned to STA. Furthermore, 2θ value of 8.08, 8.8, 17.58, 20.08, 28.36, and 38.68 was assigned to TPA (Figure 5.13).

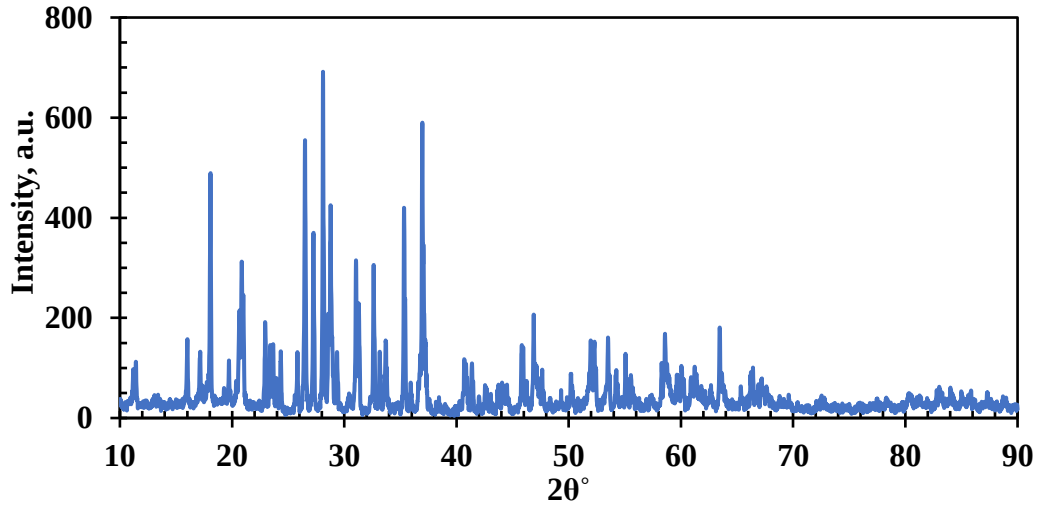

Figure 5.12. XRD pattern of STA

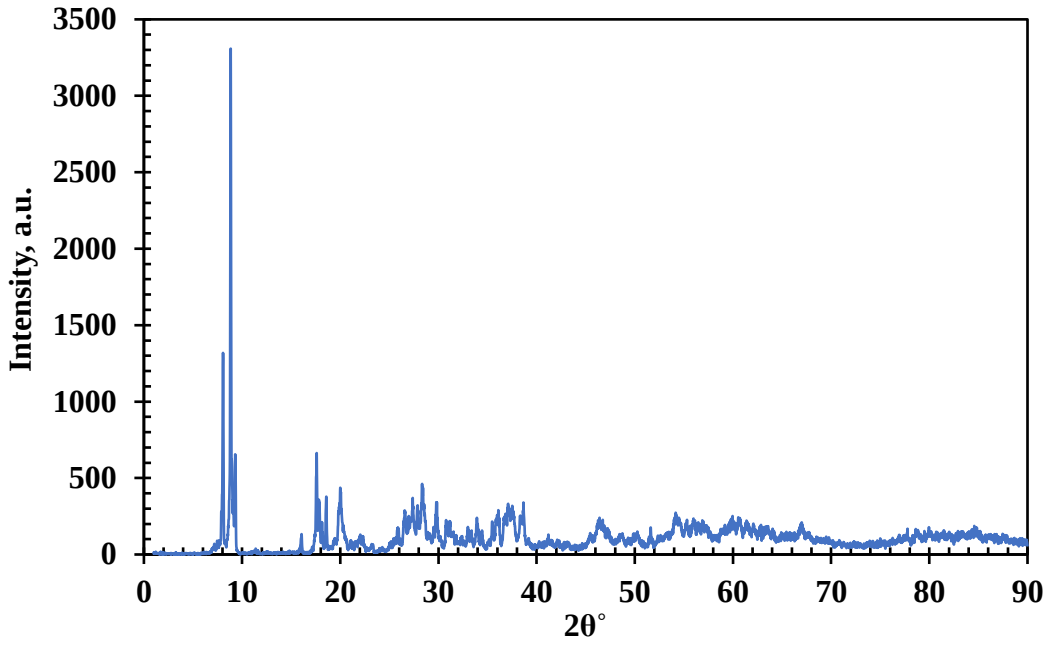

Figure 5.13. XRD pattern of TPA

Figure 5.14 demonstrates XRD patterns of different amounts of STA-loaded SA and 25% by weight of TPA-loaded SA. Because of silica aerogel's amorphous structure, silica appears as a broad peak around 22.0˚ (Musić et al., 2011; Sarıyer, M., 2018). 2θ˚ value of 10.46, 25.66, 29.68, 34.94, 37.94, 46.4, 53.64, and 60.68 peaks was observed in the SA-24STA catalyst, and these peaks belong to STA. In addition, a peak of 2θ˚ value of 35.4 was observed in the CSA-24STA catalyst. This peak belongs to STA. XRD results showed that STA is well dispersed to SA and CSA except for 24% by weight of STA-loaded SA. A peak of 2θ˚ value of 26.3 was observed in SA-25TPA, and this peak belongs to TPA. TPA is also well dispersed to SA, according to Figure 5.14.

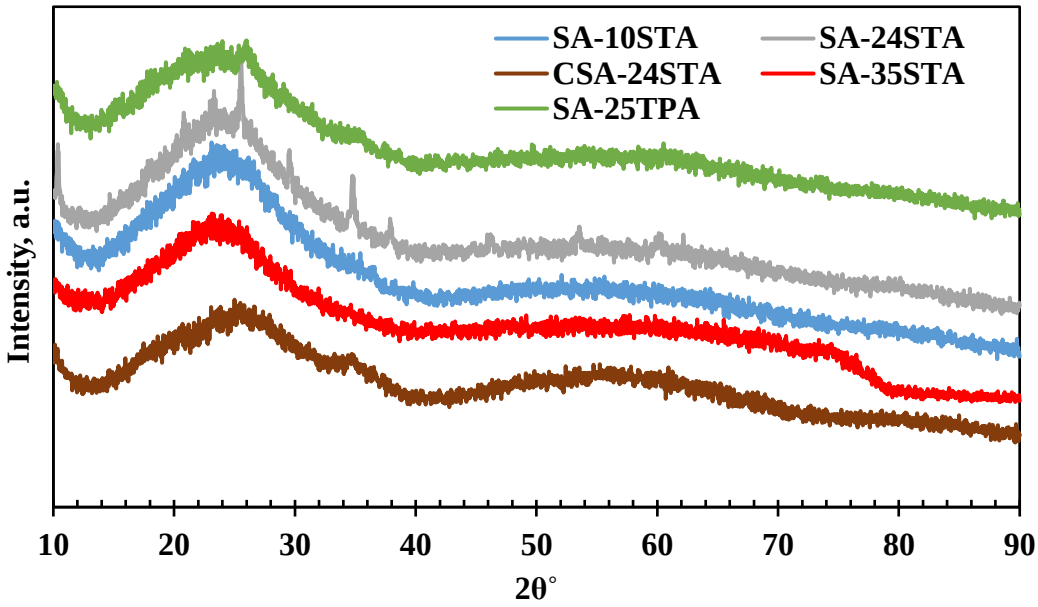

Figure 5.14. XRD patterns of different amounts of STA-loaded SA and 25% by weight of TPA-loaded SA

5.1.3 TGA Analysis

TGA analysis was performed to determine the calcination temperature of uncalcined metal-loaded silica aerogel. Figure 5.15 shows the TGA curve of uncalcined SA-24STA. In the TGA curve, physically deposited H_2O molecules on the material bring about a weight loss of 4% up to 150 ℃. From 300 ℃ to 500 ℃, the separation of water in the STA structure causes a weight loss of approximately 4%. The methyl groups (-CH_3) in SA are also cleaved above 300℃. Above 500 ℃, STA is completely decomposed into WO_3 and SiO_2 (Katryniok et al., 2012). The methyl groups (-CH_3) continue to separate from the silica aerogel structure above 500 ℃. Approximately 10.5% weight loss of SA-24STA was observed up to 900 ℃. The sequence of reactions leading to thermal decomposition of STA is given below (Katryniok et al., 2012):

$$H_4SiW_{12}O_{40}\,nH_2O \underset{<200℃}{\overset{-nH_2O}{\Longleftrightarrow}} H_4SiW_{12}O_{40} \underset{>300℃}{\overset{-2\,H_2O}{\Longleftrightarrow}} SiW_{12}O_{38} \underset{>500℃}{\Longleftrightarrow} 12\,WO_3 + Sio_2$$

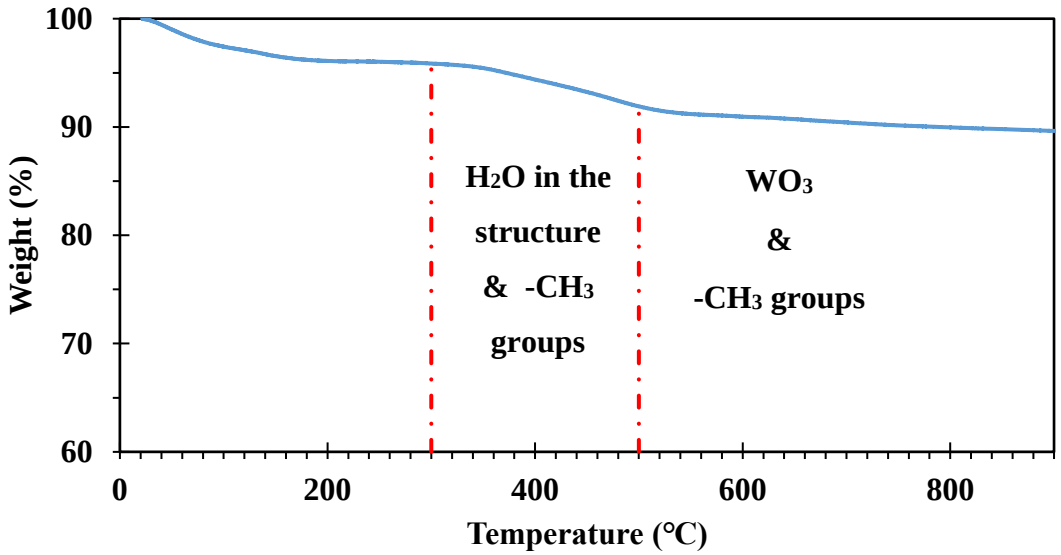

Figure 5.15. TGA curve of uncalcined SA-24STA

Calcination temperature was chosen 375℃ for the metal-loaded SA because there was no significant change in the structure of SA and STA, and there was about 5% weight loss of SA-24STA. All metal-loaded SA was calcined at 375 ℃ before reaction.

5.1.4 FTIR Analysis

Figure 5.16 shows FTIR spectra of SA and CSA. Peaks obtained in the spectrum of SA material at 759 cm^{-1} and 821 cm^{-1} are due to Si-O-Si stretching. Because of the TMCS modification, C-H stretching was detected at a wavenumber of 2963 cm^{-1}. Peaks at 847 cm^{-1} and 1256 cm^{-1} are caused by Si-C stretching. The sharp peak at 1068 cm^{-1} with a shoulder at 1146 cm^{-1} is from Si-O-Si stretching. The FTIR results revealed that SA has the typical silica aerogel peaks. The similar behavior was seen in the literature (Sivri et al., 2019).

The removal of $-CH_3$ groups during the calcination process reduced the intensities of the C-H stretching peak at 2963 cm^{-1} and the Si-C stretching peaks at 847 cm^{-1} and 1256 cm^{-1} in the CSA material. The similar behavior was seen in the literature's

other calcined silica aerogel as well (Sivri et al., 2019). This might be because of the Si-CH_3 bonds being converted to Si-OH bonds to increase the stability of the Si-O-Si structure.

A broad peak containing -OH group around 3500 cm^{-1} was detected in CSA in Figure 5.16. However, a peak around 3500 cm^{-1} was not observed in SA because SA is hydrophobic. With the removal of the -CH_3 groups in SA, the hydrophobic material became hydrophilic and the -OH group appeared in CSA.

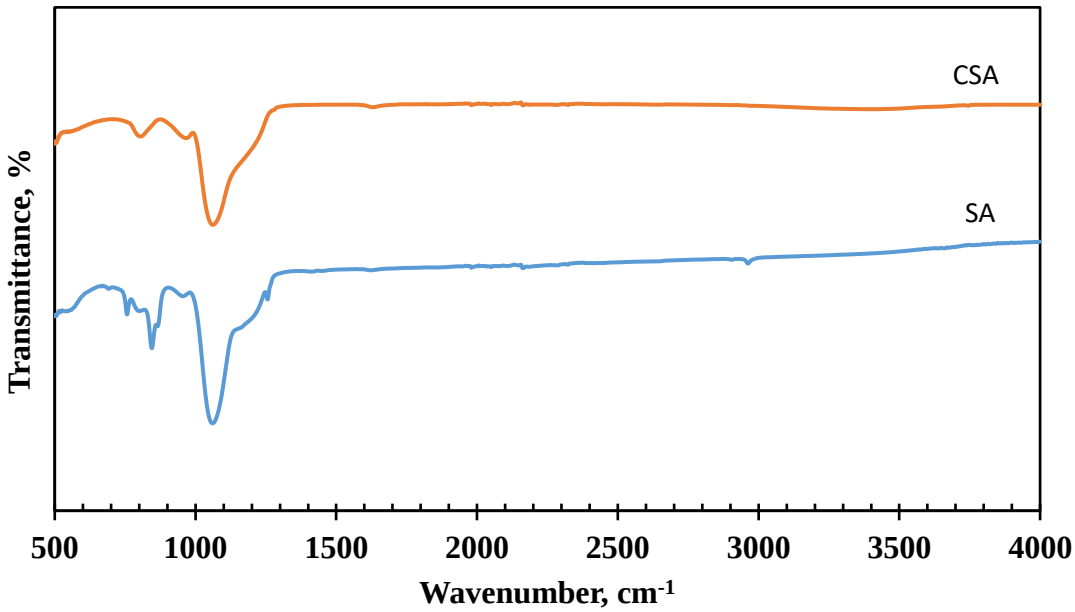

Figure 5.16. FTIR spectra of SA and CSA

5.1.5 DRIFTS Analysis

The nature of the acidity of STA and TPA loaded SA and co-loading of aluminum and STA into SA was investigated in this section using the pyridine adsorption technique. The Lewis and Brønsted acidity of the catalysts are determined using adsorption bands with wavenumbers ranging from 1400-1700 cm^{-1}. Lewis acidity is found at 1632 and 1580 cm^{-1}, around 1575 cm^{-1}, and between 1455 and 1438 cm^{-1}, whereas Brønsted acidity is found at 1640 and 1540 cm^{-1}. The band near 1490 cm^{-1}

corresponds to both Lewis and Brønsted acid sites in the material structure (Gokturk, 2021).

The nature of acidities of 10%, 24%, and 35% by weight STA loaded SA, and 25% by weight TPA loaded SA and co-loading of aluminum and STA into SA were determined using the adsorption bands wavenumbers shown in Figure 5.17.

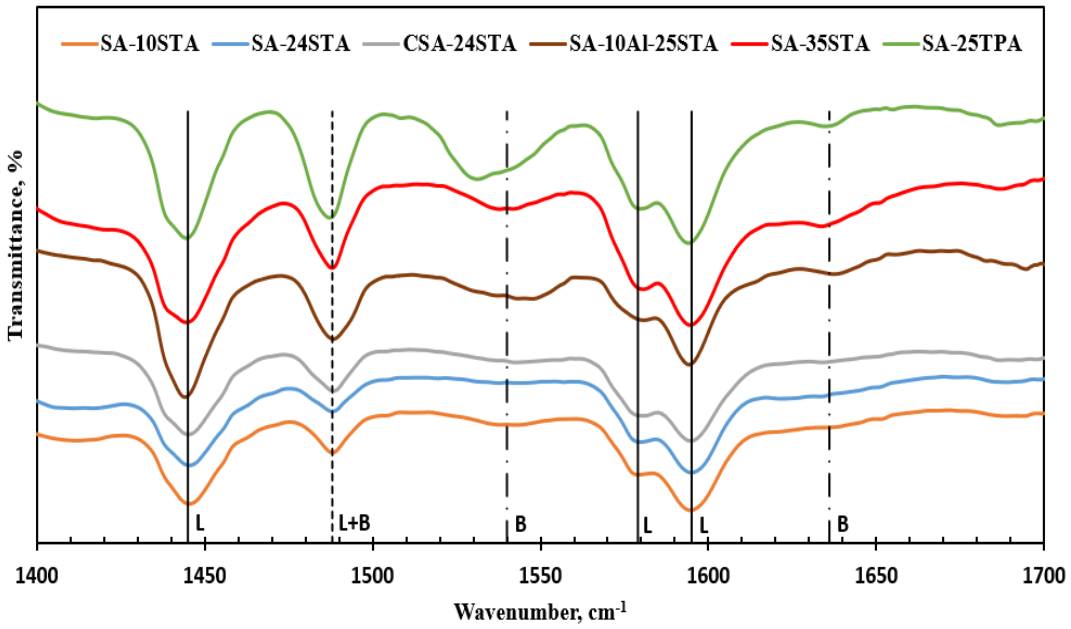

Figure 5.17. DRIFTS spectra of adsorbed pyridine on different amounts of STA-loaded SA, 25% by weight of TPA-loaded SA, and co-loading of aluminum and STA into SA

Figure 5.17 shows that all STA and TPA-loaded SA and co-loading of aluminum and STA into SA had intense bands with similar wavenumbers. The intense bands around 1595, 1579, and 1445 cm^{-1} in all catalysts correspond to Lewis acid sites, while the broadband at 1488 cm^{-1} refers to both Lewis and Brønsted acid sites. The band at 1540 and 1636 cm^{-1} refers to Brønsted acid sites.

The ratios of intensities in the Lewis site at a wavenumber of 1445 cm^{-1} to the intensities in the Brønsted site at a wavenumber of 1636 cm^{-1} in the synthesized catalysts increase in the following order:

SA-35STA < SA-24STA < SA-10STA < SA-25TPA < CSA-24STA < SA-10Al-25STA

5.2 DME Production

Catalyst performance tests were conducted using a DME production system at 275 °C and 50 bar with a total 25 ml/min CO/H_2 (1/1) flowrate. A total of 0.3 g of bifunctional catalyst mixture (MSC+CA and MSC+synthesized catalysts) was used at a 1/1 ratio by weight. The reduction procedure of the catalysts was carried out at 275 °C prior to the DME production reaction. The DME production reaction time was 5 hours. Reactor effluent streams were continuously analyzed using GC, and the outlet stream compositions were calculated using the calibration factors (Appendix B) of the components.

CO fractional conversion and product selectivities were computed (Appendix C). During the experiment, the areas of the products and reactants (H_2, CO, CO_2, CH_3OH, CH_4, DME, C_2H_5OH, and HCOOH) were taken from the GC pictogram every 50 minutes, and number of moles of components were calculated. The experiment reached a steady state at the 150^{th} minute. Therefore, the last four data points where the system reached a steady state were used to calculate the average conversion and selectivity values.

5.2.1 Repeatability Tests

At 275 °C and 50 bar over MSC and CA (1/1 wt. ratio) catalysts, DME production experiments were carried out three times at different times. The chemical composition of the reactor stream was determined using GC analysis. In addition to carbon monoxide and hydrogen gases, CH_4, CO_2, HCOOH (formic acid), CH_3OH (methanol), DME, and C_2H_5OH (ethanol) were detected as products in the reactor's effluent stream. Methanol and CH_4 are formed from CO hydrogenation R1 and R9

reactions, respectively. DME is formed from a methanol dehydration reaction (R3). WGSR causes the formation of CO_2 (R4).

$$CO + 2H_2 \rightleftharpoons CH_3OH \quad \text{(R1)}$$

$$CO_2 + 3H_2 \rightleftharpoons CH_3OH + H_2O \quad \text{(R2)}$$

$$2CH_3OH \rightleftharpoons CH_3OCH_3 + H_2O \quad \text{(R3)}$$

$$H_2O + CO \rightleftharpoons H_2 + CO_2 \quad \text{(R4)}$$

$$CO_2 + H_2 \rightleftharpoons HCOOH \quad \text{(R7)}$$

$$2CO + 4H_2 \rightleftharpoons C_2H_5OH + H_2O \quad \text{(R8)}$$

$$CO + 3H_2 \rightleftharpoons CH_4 + H_2O \quad \text{(R9)}$$

Trace amounts of formic acid and ethanol, which are formed from CO_2 and CO hydrogenation R7 and R8 reactions, respectively, were also observed, along with the main products methane, carbon dioxide, methanol and dimethyl ether. Therefore, the selectivities of these products not shown in figures unless otherwise stated.

DME production experiments were carried out with a mixture of MSC and CA catalysts with a weight ratio of 1/1 at 275 °C, and 50 bar pressure. The average conversion as a function of time for these three replicates are given in Figure 5.18 with standard deviation.

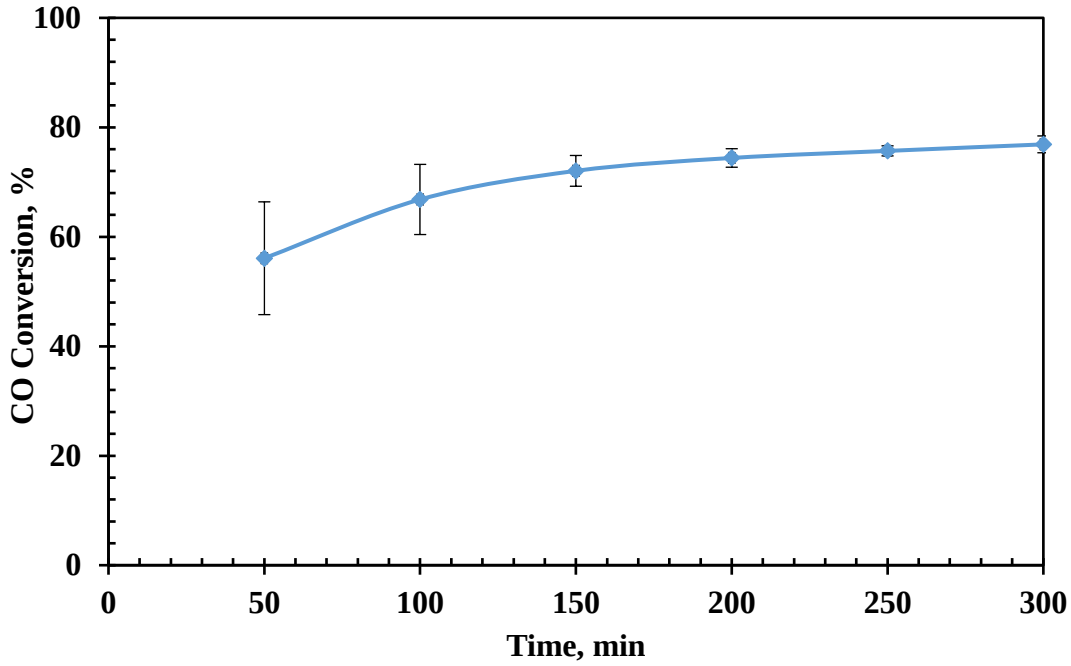

Figure 5.18. Average CO conversion of three runs with respect to time for DME production with standard deviation (P=50 bar, T=275 °C, CO/H_2=1/1, MSC/CA catalyst: 1/1)

According to Figure 5.18, the system reaches the steady state within 150 minutes. After reaching the steady state, the average of the last four data was calculated. It was calculated in the same way for the other two experiments performed at different times. The results of the three different experiments calculated were averaged and the standard deviation of these values was calculated. The average CO conversion of the three experiments was found to be 74.8% with a standard deviation of 1.7 points. These results showed that data are consistent with each other. In other words, the experiments are repeatable and reliable.

Figure 5.19 shows average product distribution of three runs with standard deviation. According to Figure 5.19, the maximum standard deviation is 2.5. Average mole fractions of DME, CO_2, MeOH, CH_4, FA, and EtOH were 34.5%, 56.6% 3.0%, 3.7%, 1.6%, and 0.67%, respectively.

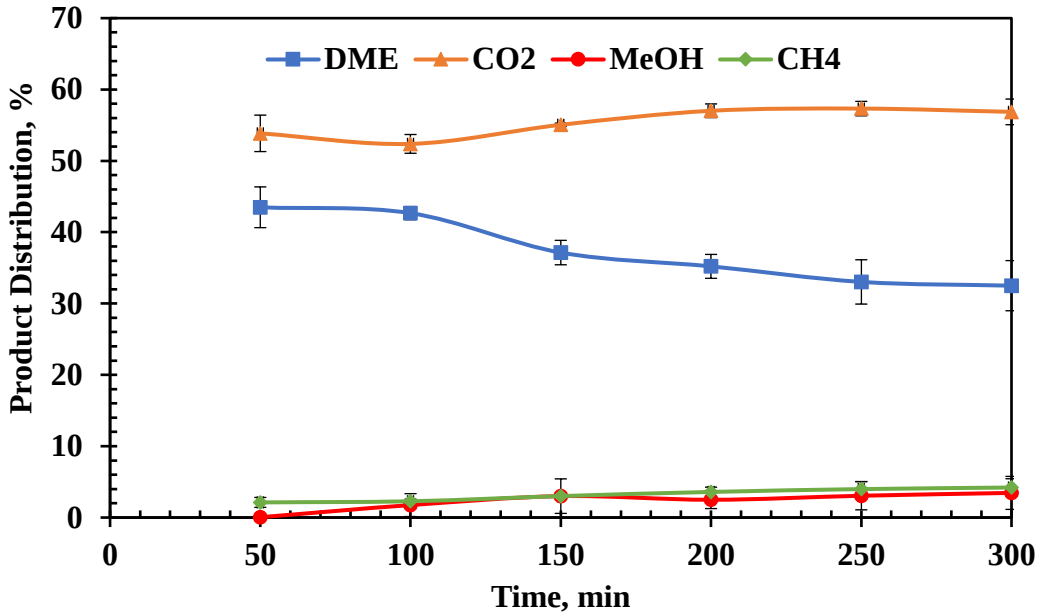

Figure 5.19. The product distribution of three runs with respect to time (P=50 bar, T=275 °C, CO/H_2=1/1, MSC/CA catalyst: 1/1)

Figure 5.20 demonstrates the average product selectivities of three runs with a standard deviation. Product selectivity results were similar in all three experiments. The average DME selectivity was 50.9%, while the average CO_2 selectivity was around 41.9%. In addition, the average selectivity of ethanol and formic acid was around 1%. The maximum standard deviation for all three-test results was less than 2.8%.

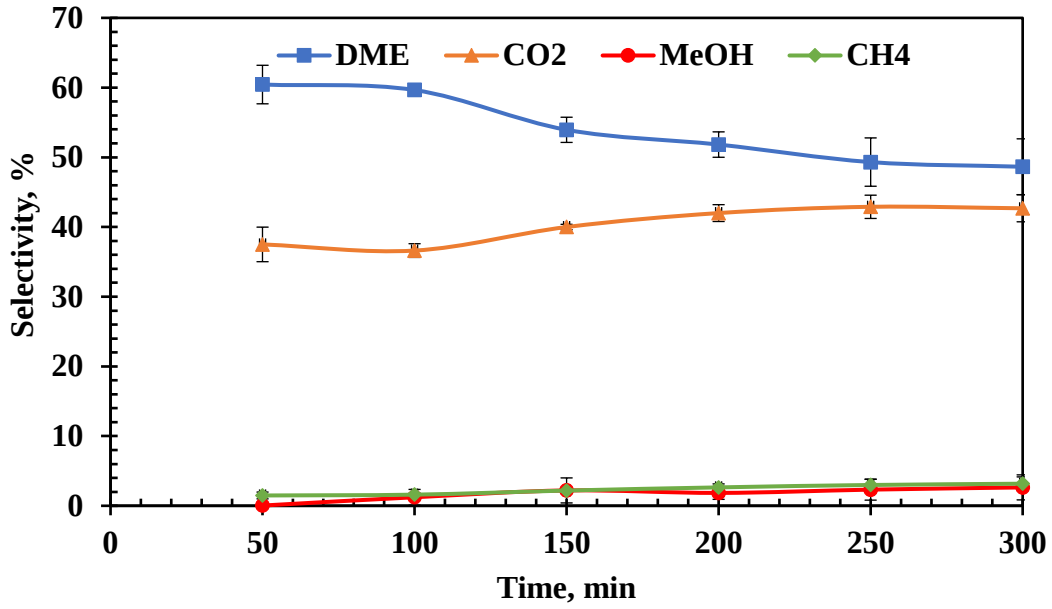

Figure 5.20. Product selectivities of three runs with respect to time (P=50 bar, T=275 °C, CO/H_2=1/1, MSC/CA catalyst: 1/1)

5.2.2 Effect of Metal Loading into Support on DME Production

The effect of different amounts of metal-loaded support on DME production is explained in this section. DME selectivities were also investigated.

5.2.2.1 Effect of STA Amount

STA was impregnated into SA support with different amount. Synthesized catalysts were mixed physically with CA in the activity tests. The effect of STA amount on CO conversion and product selectivities was investigated. In addition to carbon monoxide and hydrogen gases, CH_4, CO_2, HCOOH, CH_3OH, DME, and C_2H_5OH were detected as products in the reactor's effluent stream.

Three different STA amounts (10%, 24%, and 35% by weight) were impregnated on SA support. The average CO conversion and product selectivities are depicted in Figure 5.21. The CO conversion increased from 62% to 68.8% when the amount of

STA was increased from 10% to 24%. When the STA amount was increased to 35%, the conversion decreased 66.14% slightly. The highest CO conversion was obtained in the catalyst loaded with 24% STA.

When the amount of STA increased from 10% to 24%, its selectivity increased from 42.1% to 42.9%. When the STA amount was increased to 35%, the DME selectivity reached 50.6%. It was observed that the DME selectivity increased as the amount of STA increased.

The ethanol selectivities of SA-10STA, SA-24STA and SA-35 STA were 2%, 2.1% and 1%, respectively, while the formic acid selectivities of SA-10STA, SA-24STA and SA-35 STA were 2.4%, 2.4%, and 2%, respectively. SA-10STA, SA-24STA, and SA-35STA had methane selectivities of 4.5%, 3%, and 3.6%, respectively.

DRIFTS results showed that Brønsted acid sites in the catalyst increased as the amount of STA increased. Increasing the Brønsted acid sites gave better DME selectivity. With an increase in Brønsted acid sites DME yield increased as shown in Figure 5.22. It can be said that almost all of the methanol produced is used because there is almost no methanol.

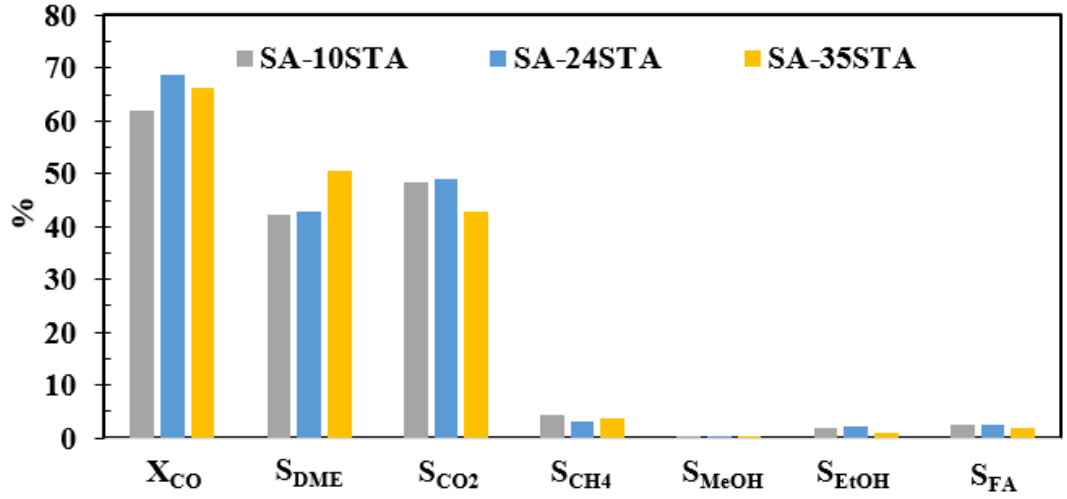

Figure 5.21. Effect of STA amount impregnated to SA support on CO conversion and product selectivities (P=50 bar, T=275 °C, CO/H_2=1/1, MSC/synthesized catalyst: 1/1 (wt.))

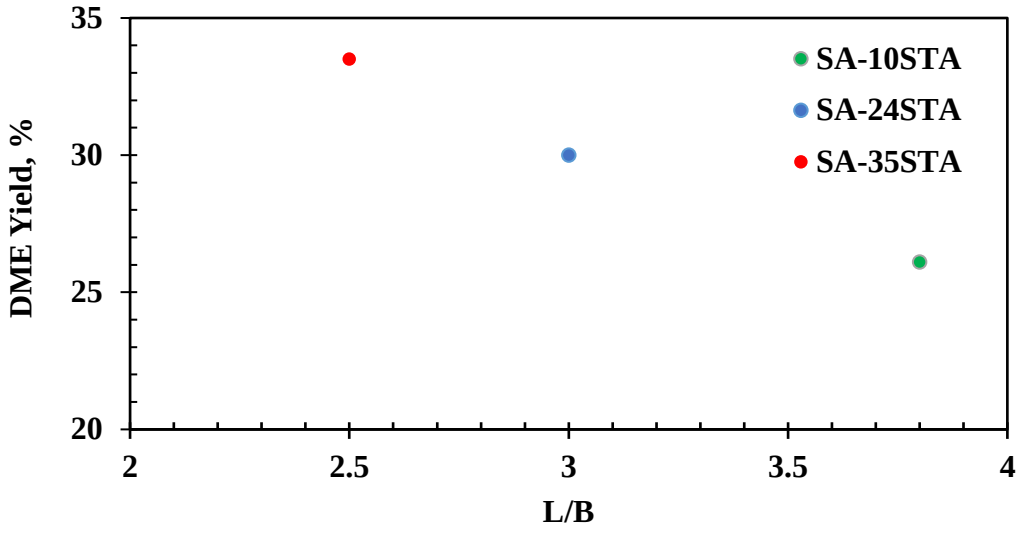

Figure 5.22. Effect of L/B on DME yield

Figure 5.23 shows that CO conversion value obtained using MSC+SA-35STA catalyst and the equilibrium conversion values at different temperature. The CO conversion with the MSC+SA-35STA catalyst is lower than the equilibrium CO conversion.

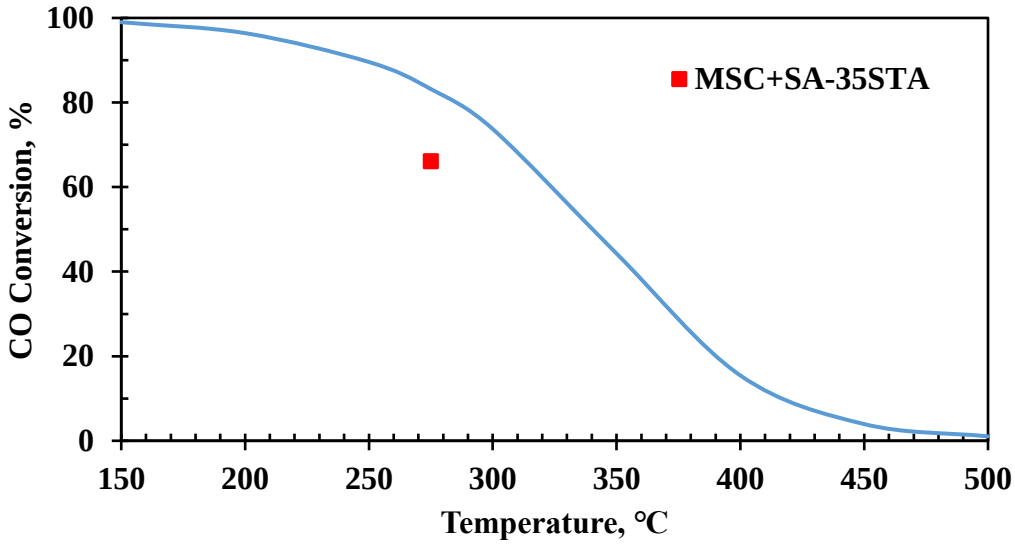

Figure 5.23. Comparison of CO conversion values obtained using the MSC+SA-35STA catalyst with equilibrium conversion values at 50 bar, 275 °C and with CO/H_2=1/1

5.2.2.2 Effect of STA Loaded Calcined and Uncalcined SA on DME Production

Figure 5.24 shows the effect of calcined and uncalcined SA support on DME production. Impregnation of STA on CSA yielded higher CO conversion (79.5%), while DME and CO_2 selectivity were very close to each other. The multipoint BET surface area and pore diameter of SA-24STA and CSA-24STA were too close to each other, and DME selectivity values were the same as CSA-24STA, which had fewer Brønsted acid sites, although SA-24STA had more Brønsted acid sites. This may be due to the better distribution of STA in the calcined support material (Figure 5.14).

The CH_4 selectivity of SA-24STA and CSA-24STA was 3% and 4.3%, respectively. The ethanol selectivity of SA-24STA and CSA-24STA was 2.1% and 2.3%, respectively, whereas SA-24STA and CSA-24STA's formic acid selectivities were 2.4% and 2.8%, respectively.

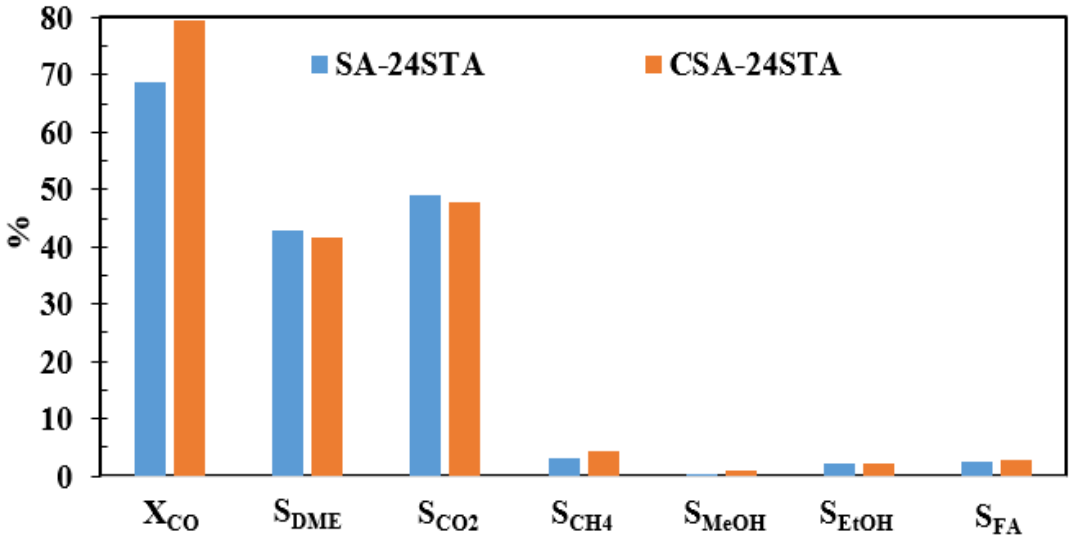

Figure 5.24. The effect of calcined and uncalcined SA support on DME production (P=50 bar, T=275 °C, CO/H_2=1/1, MSC/synthesized catalyst: 1/1 (wt.))

5.2.2.3 Comparison of the Synthesized Catalysts

The average CO conversion and product selectivities of metal-loaded SA support and CA catalysts are given in Figure 5.25.

The SA-10Al-25STA catalyst gave the lowest CO conversion, while the commercial alumina catalyst gave the highest CO conversion. The highest DME selectivity was obtained with SA-35STA and commercial alumina, while SA-25TPA gave the lowest DME selectivity. Commercial alumina and SA-25TPA gave the lowest and highest methane selectivity, respectively. Whereas SA-35STA and commercial alumina gave the lowest ethanol selectivity, SA-25TPA gave the highest one. In addition, the lowest and highest formic acid selectivity was obtained with commercial alumina and SA-25TPA, respectively.

The average CO conversion values are approximately the same for the catalyst SA-24STA and SA-25TPA catalyst (Figures 5.21 and 5.25). Although the average CO conversion values of the SA-24STA and SA-25TPA catalysts were close to each other, the DME selectivity of SA-25TPA was significantly reduced. SA-25TPA had a DME selectivity of 16.7%. On the other hand, the CH_4 selectivity of SA-24STA and SA-25TPA is 3% and 14.3%, respectively. In addition, SA-25TPA catalyst gave higher ethanol and formic acid selectivity, 6.64% and 8.43%, respectively, than SA-24STA.

The SA-10Al-25STA catalyst had lower Brønsted acid sites than the SA-35STA catalyst, resulting in lower DME selectivity as seen in Figure 5.25. According to Figures 5.24 and 5.25, the higher DME selectivity of the SA-10Al-25STA catalyst than SA-24STA may be due to 10% more metal loading and better STA interaction with alumina.

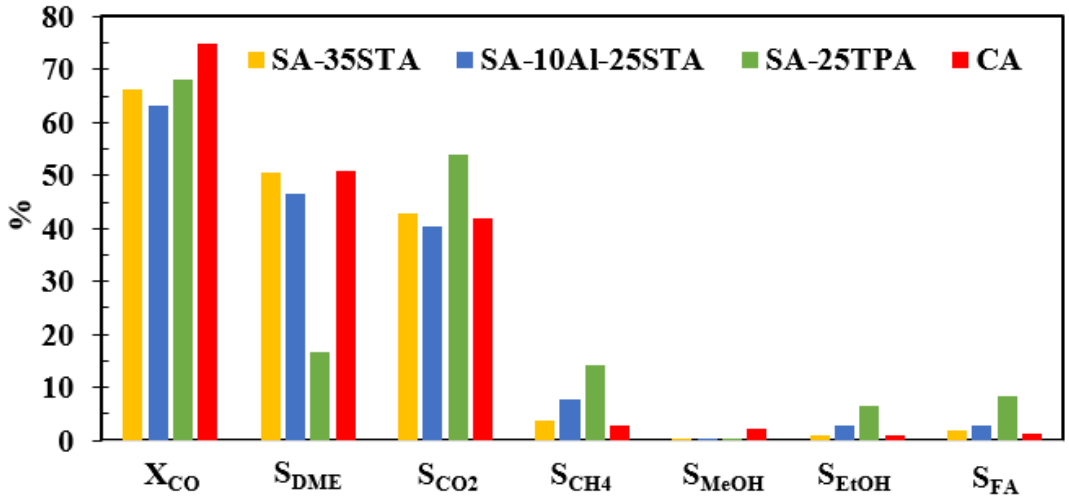

Figure 5.25. Comparison of the synthesized catalysts (P=50 bar, T=275 °C, CO/H_2=1/1, MSC/synthesized catalyst or CA: 1/1 (wt.))

According to Figure 5.24 and 5.25, the CO conversion of 24% STA loaded on SA was close to 25% TPA loaded on SA. DME selectivity of SA-24STA had higher than that of SA-25TPA despite higher multipoint BET surface area and BJH desorption pore size of SA-25TPA catalyst. SA-25TPA had lower Brønsted acid sites than SA-24STA and SA-35STA, DME selectivity was reduced. The higher Lewis acid sites on the SA-25TPA catalyst compared to SA-24STA and SA-35STA caused methane, ethanol and formic acid reactions to occur and their selectivity increased.

While in one study, 63.1% DME selectivity with 39% CO conversion was obtained in DME production at 275 °C and 50 bar using 30STA@CZA:631 catalyst (Pekmezci Karaman et al., 2020), the DME selectivity of the best catalyst in this study (SA-35STA) was 50.6%, and although DME selectivity is lower than that of literature, the CO conversion, 66.1%, was higher than that of Pekmezci's study. In other words, the DME yield (33.5%) of the best catalyst is higher than that of Pekmezci's study.

In another study, 49% CO conversion and 16% DME selectivity were obtained with 25% TPA impregnated synthesized mesoporous alumina (EMA) catalyst (Sener, 2019). The DME selectivity of the SA-25TPA catalyst in this study was close to that

of the literature. However, the CO conversion was higher than that of the literature. It had been observed that the silica aerogel support material had a higher multipoint BET surface area (793 m^2/g) than that of the mesoporous alumina support material (256 m^2/g) which had a positive effect on the CO conversion.

As a result, among the synthesized catalysts, the SA-35STA catalyst had the highest DME selectivity. The DME yield of SA-35STA was found to be 33.5%. DME selectivity of SA-35STA was also close to commercial alumina catalyst' selectivity and yield (50.9% and 38%, respectively), and SA-35STA catalyst can be used in place of commercial alumina catalyst. Therefore, it was observed that SA-35STA together with MSC is a suitable catalyst candidate for direct DME synthesis.

CHAPTER 6

CONCLUSIONS AND RECOMMENDATIONS

In this study, silica aerogel support material was synthesized by sol-gel synthesis method. STA, TPA and alumina were loaded on the silica aerogel support material by impregnation method. Nitrogen physisorption technique, XRD, TGA, FTIR, and DRIFTS were used to characterize the synthesized material. The synthesized catalysts and commercial alumina catalyst were physically mixed with commercial methanol catalyst and used in activity tests for DME production at 275 ℃ and 50 bar in a fixed bed reactor. The following results were obtained:

- Silica aerogel support materials were synthesized via the sol-gel method, demonstrating Type IV isotherms with H3 type hysteresis loop, indicating mesoporous structure. The multipoint BET surface area, BJH desorption average pore diameter, and BJH desorption cumulative pore volume of SA were 793±14.1 m^2/g, 10.9±0.4 nm, and 3.44±0.09 cm^3/g, respectively. SA was an amorphous structure.
- The metals loading into SA support material altered the hysteresis loop to H1, whereas the isotherm type kept the same, representing Type IV. The mesoporous structure property did not change. In addition, increasing the amount of STA in SA support material decreased the surface area of the synthesized catalysts due to clogging of pores.
- At various pressures and temperatures, thermodynamic equilibrium studies were carried out. Based on the equilibrium studies, a pressure of 50 bar, a temperature of 275 °C and a CO/H_2 molar ratio of 1/1 were chosen.
- L/B ratios in the synthesized catalysts increase in the following order:

  SA-35STA < SA-24STA < SA-10STA < SA-25TPA < CSA-24STA < SA-10Al-25STA

- Commercial methanol synthesis (MSC) and commercial alumina (CA) catalyst mixture had the highest DME selectivity 50.9% with the 74.8% CO conversion.
- Brønsted acid sites increased as the amount of STA increased, which increased the DME selectivity.
- As a result of the experiments conducted under the aforementioned operating conditions, the best catalyst synthesized in this study was determined as SA-35STA. In the presence of this catalyst, 66.1% CO conversion and 50.6% DME selectivity were obtained. The DME yield of SA-35STA was found to be 33.5%. The SA-35STA catalyst can be used in place of commercial alumina catalyst because its DME selectivity (50.9%) is comparable to that of commercial alumina catalyst. Therefore, it was observed that SA-35STA together with MSC is a suitable catalyst candidate for direct DME synthesis.

It is recommended to use synthesized catalysts at temperatures between 200 and 275 °C and 50 bar. Furthermore, the bifunctional catalyst obtained by simultaneous loading of copper and STA on silica aerogel is recommended for use in direct DME synthesis. For the reusability of this experiment, long-term reaction experiments are recommended. It is also recommended to synthesize DME by adding CO_2 to CO/H_2 gases.

REFERENCES

Ahmad, R., Schrempp, D., Behrens, S., Sauer, J., Döring, M., & Arnold, U. (2014). Zeolite-based bifunctional catalysts for the single step synthesis of dimethyl ether from CO-rich synthesis gas. *Fuel Processing Technology*, *121*, 38–46. https://doi.org/10.1016/j.fuproc.2014.01.006

Ali, K. A., Abdullah, A. Z., & Mohamed, A. R. (2015). Recent development in catalytic technologies for methanol synthesis from renewable sources: A critical review. *Renewable and Sustainable Energy Reviews*, *44*, 508–518. https://doi.org/10.1016/j.rser.2015.01.010

Azizi, Z., Rezaeimanesh, M., Tohidian, T., & Rahimpour, M. R. (2014). Dimethyl ether: A review of technologies and production challenges. *Chemical Engineering and Processing: Process Intensification*, *82*, 150–172. https://doi.org/10.1016/j.cep.2014.06.007

Bayat, A., & Dogu, T. (2016). Optimization of CO_2/CO Ratio and Temperature for Dimethyl Ether Synthesis from Syngas over a New Bifunctional Catalyst Pair Containing Heteropolyacid Impregnated Mesoporous Alumina. *Industrial and Engineering Chemistry Research*, *55*(44), 11431–11439. https://doi.org/10.1021/acs.iecr.6b03001

Cai, M., Palčić, A., Subramanian, V., Moldovan, S., Ersen, O., Valtchev, V., Ordomsky, V. V., & Khodakov, A. Y. (2016). Direct dimethyl ether synthesis from syngas on copper-zeolite hybrid catalysts with a wide range of zeolite particle sizes Dedicated to Professor Jean-Pierre Gilson on the occasion of his 60th birthday. *Journal of Catalysis*, *338*, 227–238. https://doi.org/10.1016/j.jcat.2016.02.025

Celik, G., Arinan, A., Bayat, A., Ozbelge, H. O., Dogu, T., & Varisli, D. (2013). Performance of silicotungstic acid incorporated mesoporous catalyst in direct synthesis of dimethyl ether from syngas in the presence and absence of CO_2. *Topics in Catalysis*, *56*(18–20), 1764–1774. https://doi.org/10.1007/s11244-013-0112-4

Ciftci, A., Varisli, D., & Dogu, T. (2010). Dimethyl ether synthesis over novel silicotungstic acid incorporated nanostructured catalysts. *International Journal of Chemical Reactor Engineering*, *8*(1). https://doi.org/10.2202/1542-6580.2151

Ciftci, A., Varisli, D., Tokay, K. C., Sezgi, N. A., & Dogu, T. (2012). Dimethyl ether, diethyl ether & ethylene from alcohols over tungstophosphoric acid based mesoporous catalysts. *Chemical Engineering Journal*, *207–208*, 85–93. https://doi.org/10.1016/j.cej.2012.04.016

García-Trenco, A., & Martínez, A. (2012). Applied Catalysis A : General Direct

synthesis of DME from syngas on hybrid CuZnAl / ZSM-5 catalysts : New insights into the role of zeolite acidity. *"Applied Catalysis A, General," 411–412*, 170–179. https://doi.org/10.1016/j.apcata.2011.10.036

García-Trenco, A., Valencia, S., & Martínez, A. (2013). The impact of zeolite pore structure on the catalytic behavior of CuZnAl/zeolite hybrid catalysts for the direct DME synthesis. *Applied Catalysis A: General*, *468*, 102–111. https://doi.org/10.1016/j.apcata.2013.08.038

Gokturk, S. (2021). Hydrogen Production via Steam Reforming of Glycerol Master of Science. Middle East Technical University, Ankara, Türkiye.

Gurav, J. L., Jung, I. K., Park, H. H., Kang, E. S., & Nadargi, D. Y. (2010). Silica aerogel: Synthesis and applications. *Journal of Nanomaterials*, *2010*. https://doi.org/10.1155/2010/409310

Hamed Bateni, & Chad Able. (2019). Development of Heterogeneous Catalysts for Dehydration of Methanol to Dimethyl Ether: A Review. *Catalysis in Industry*, *11*(1), 7–33. https://doi.org/10.1134/S2070050419010045

Jansen, S. A., Wang, S. H., & Eddowes, A. D. (1997). Stability and acidity contributions of heteropolymetalates: a theoretical study of the Keggin and Dawson ions. *Supramolecular Science*, *4*(1–2), 51–58. https://doi.org/10.1016/S0968-5677(96)00058-2

Katryniok, B., Paul, S., Capron, M., Bellière-Baca, V., Rey, P., & Dumeignil, F. (2012). Regeneration of silica-supported silicotungstic acid as a catalyst for the dehydration of glycerol. *ChemSusChem*, *5*(7), 1298–1306. https://doi.org/10.1002/cssc.201100635

Lange, J. P. (2001). Methanol synthesis: A short review of technology improvements. *Catalysis Today*, *64*(1–2), 3–8. https://doi.org/10.1016/S0920-5861(00)00503-4

Li, F., Ao, M., Hung Pham, G., Jin, Y., Hoang Nguyen, M., Majd Alawi, N., Tade, M. O., & Liu, S. (2020). A novel UiO-66 encapsulated 12-silicotungstic acid catalyst for dimethyl ether synthesis from syngas. *Catalysis Today*, *355*, 3–9. https://doi.org/10.1016/j.cattod.2019.07.057

Liu, X. M., Lu, G. Q., Yan, Z. F., & Beltramini, J. (2003). Recent Advances in Catalysts for Methanol Synthesis via Hydrogenation of CO and CO_2. *Industrial and Engineering Chemistry Research*, *42*(25), 6518–6530. https://doi.org/10.1021/ie020979s

Maleki, H., Durães, L., & Portugal, A. (2014). An overview on silica aerogels synthesis and different mechanical reinforcing strategies. *Journal of Non-Crystalline Solids*, *385*, 55–74. https://doi.org/10.1016/j.jnoncrysol.2013.10.017

Millán, E., Mota, N., Guil-López, R., Pawelec, B., Fierro, J. L. G., & Navarro, R. M.

(2020). Direct synthesis of dimethyl ether from syngas on bifunctional hybrid catalysts based on supported $H_3PW_{12}O_{40}$ and Cu-ZnO(Al): Effect of heteropolyacid loading on hybrid structure and catalytic activity. *Catalysts*, *10*(9), 1–22. https://doi.org/10.3390/catal10091071

Mondal, U., & Yadav, G. D. (2019). Perspective of dimethyl ether as fuel: Part I. Catalysis. *Journal of CO_2 Utilization*, *32*, 299–320. https://doi.org/10.1016/j.jcou.2019.02.003

Musić, S., Filipović-Vinceković, N., & Sekovanić, L. (2011). Precipitation of amorphous SiO_2 particles and their properties. *Brazilian Journal of Chemical Engineering*, *28*(1), 89–94. https://doi.org/10.1590/S0104-66322011000100011

Peinado, C., Liuzzi, D., Ladera-Gallardo, R. M., Retuerto, M., Ojeda, M., Peña, M. A., & Rojas, S. (2020). Effects of support and reaction pressure for the synthesis of dimethyl ether over heteropolyacid catalysts. *Scientific Reports*, *10*(1), 1–12. https://doi.org/10.1038/s41598-020-65296-3

Pekmezci Karaman, B., & Oktar, N. (2020). Tungstophosphoric acid incorporated hierarchical HZSM-5 catalysts for direct synthesis of dimethyl ether. *International Journal of Hydrogen Energy*, *45*(60), 34793–34804. https://doi.org/10.1016/j.ijhydene.2020.07.044

Pekmezci Karaman, B., Oktar, N., Doğu, G., & Doğu, T. (2020). Bifunctional Silicotungstic Acid and Tungstophosphoric Acid Impregnated Cu–Zn–Al & Cu–Zn–Zr Catalysts for Dimethyl Ether Synthesis from Syngas. *Catalysis Letters*, *150*(9), 2744–2761. https://doi.org/10.1007/s10562-020-03171-6

Rao, A. P., Rao, A. V., & Pajonk, G. M. (2005). Hydrophobic and physical properties of the two step processed ambient pressure dried silica aerogels with various exchanging solvents. *Journal of Sol-Gel Science and Technology*, *36*(3), 285–292. https://doi.org/10.1007/s10971-005-4662-1

Rostrup-Nielsen, J. R. (2000). New aspects of syngas production and use. *Catalysis Today*, *63*(2–4), 159–164. https://doi.org/10.1016/S0920-5861(00)00455-7

Saravanan, K., Ham, H., Tsubaki, N., & Bae, J. W. (2017). Recent progress for direct synthesis of dimethyl ether from syngas on the heterogeneous bifunctional hybrid catalysts. *Applied Catalysis B: Environmental*, *217*, 494–522. https://doi.org/10.1016/j.apcatb.2017.05.085

Sarıyer, M. (2018). Sorption enhanced reforming of ethanol over novel catalysts and microwave reactor application Master of Science. Middle East Technical University, Ankara, Türkiye.

Sener, M. I. (2019). Development of Bifunctional Catalyst for the Single-step Synthesis of Dimethyl Ether Master of Science. Middle East Technical University, Ankara, Türkiye.

Shammut, M., Cao, M., Zhang, Y., Papaix, C., Liu, Y., & Gao, X. (2019). Banning diesel vehicles in London: Is 2040 too late? *Energies*, *12*(18). https://doi.org/10.3390/en12183495

Siva Kumar, V., Padmasri, A. H., Satyanarayana, C. V. V., Ajit Kumar Reddy, I., David Raju, B., & Rama Rao, K. S. (2006). Nature and mode of addition of phosphate precursor in the synthesis of aluminum phosphate and its influence on methanol dehydration to dimethyl ether. *Catalysis Communications*, *7*(10), 745–751. https://doi.org/10.1016/j.catcom.2006.02.025

Sivri, S., Dilek, C., & Sezgi, N. A. (2019). Synthesis and characterization of aluminum containing silica aerogel catalysts for degradation of PLA. *International Journal of Chemical Reactor Engineering*, *17*(5), 1–10. https://doi.org/10.1515/ijcre-2018-0163

Soleimani Dorcheh, A., & Abbasi, M. H. (2008). Silica aerogel; synthesis, properties and characterization. *Journal of Materials Processing Technology*, *199*(1), 10–26. https://doi.org/10.1016/j.jmatprotec.2007.10.060

Sorenson, S. C. (2001). Dimethyl ether in diesel engines: Progress and perspectives. *Journal of Engineering for Gas Turbines and Power*, *123*(3), 652–658. https://doi.org/10.1115/1.1370373

Su, J., & Chen, J. S. (2017). Synthetic porous materials applied in hydrogenation reactions. *Microporous and Mesoporous Materials*, *237*, 246–259. https://doi.org/10.1016/j.micromeso.2016.09.039

Thapliyal, P. C., & Singh, K. (2014). Aerogels as Promising Thermal Insulating Materials: An Overview. *Journal of Materials*, *2014*, 1–10. https://doi.org/10.1155/2014/127049

Thommes, M., & Cychosz, K. A. (2014). Physical adsorption characterization of nanoporous materials: Progress and challenges. *Adsorption*, *20*(2–3), 233–250. https://doi.org/10.1007/s10450-014-9606-z

Tokay, K. C., Dogu, T., & Dogu, G. (2012). Dimethyl ether synthesis over alumina based catalysts. *Chemical Engineering Journal*, *184*, 278–285. https://doi.org/10.1016/j.cej.2011.12.034

Varıslı, D. (2007). Kinetic studies for dimethyl ether and diethyl ether production Doctor of Philosophy. Middle East Technical University, Ankara, Türkiye.

Wang, Y., Chen, Y., Yu, F., Pan, D., Fan, B., Ma, J., & Li, R. (2016). One-step synthesis of dimethyl ether from syngas on ordered mesoporous copper incorporated alumina. *Journal of Energy Chemistry*, *25*(5), 775–781. https://doi.org/10.1016/j.jechem.2016.04.014

Wang, Y., Wang, W. L., Chen, Y. X., Zheng, J. J., & Li, R. F. (2013). Synthesis of dimethyl ether from syngas using a hierarchically porous composite zeolite as the methanol dehydration catalyst. *Ranliao Huaxue Xuebao/Journal of Fuel*

Chemistry and Technology, *41*(7), 875–882. https://doi.org/10.1016/s1872-5813(13)60037-7

Wu, G., Yu, Y., Cheng, X., & Zhang, Y. (2011). Preparation and surface modification mechanism of silica aerogels via ambient pressure drying. *Materials Chemistry and Physics*, *129*(1–2), 308–314. https://doi.org/10.1016/j.matchemphys.2011.04.003

Yan, W., Wen-li, W., Yue-xian, C., Jia-jun, Z., & Rui-feng, L. I. (2013). Synthesis of dimethyl ether from syngas using a hierarchically porous composite zeolite as the methanol dehydration catalyst. *Journal of Fuel Chemistry and Technology*, *41*(7), 873–880. https://doi.org/10.1016/S1872-5813(13)60037-7

Yaripour, F., Baghaei, F., Schmidt, I., & Perregaarad, J. (2005). Synthesis of dimethyl ether from methanol over aluminium phosphate and silica-titania catalysts. *Catalysis Communications*, *6*(8), 542–549. https://doi.org/10.1016/j.catcom.2005.05.003

APPENDICES

A. XRD Data of Some Metals and Metal Oxides

XRD data of Al_2O_3, Cu, CuO, Cu_2O, Zn, and ZnO were given in Tables A.1-A.6, respectively.

Table A.1 XRD data for γ-alumina

Compound Name: Aluminum Oxide **Chemical Formula:** Al_2O_3 **PDF Card No:** 00-056-0457 **Radiation:** $CuK_{\alpha 1}$ **Wavelength:** 1.5405 Å			
2θ (°)	**d spacing (Å)**	**Intensity (%)**	**h k l**
31.97	2.80	2	2 2 0
37.68	2.38	4	3 1 1
39.43	2.28	60	2 2 2
45.84	1.98	64	4 0 0
50.23	1.81	1	3 3 1
56.98	1.61	1	4 2 2
60.79	1.52	5	5 1 1
66.85	1.40	100	4 4 0
70.34	1.34	2	5 3 1
71.49	1.32	1	4 4 2
76.02	1.25	1	6 2 0
79.36	1.21	4	5 3 3
80.46	1.19	33	6 2 2
84.85	1.14	26	4 4 4
93.55	1.06	1	6 4 2
102.34	0.99	13	8 0 0
105.70	0.97	3	7 3 3
114.98	0.91	5	7 5 1
116.18	0.91	6	6 6 2

Table A.2 XRD data for copper

Compound Name: Copper **Chemical Formula:** Cu **PDF Card No:** 00-004-0836 **Radiation:** $CuK_{\alpha 1}$ **Wavelength:** 1.5405 Å			
2θ (°)	**d spacing (Å)**	**Intensity (%)**	**h k l**
43.30	2.09	100	1 1 1
50.43	1.81	46	2 0 0
74.13	1.28	20	2 2 0
89.93	1.09	17	3 1 1
95.14	1.04	5	2 2 2
116.92	0.90	3	4 0 0
136.51	0.83	9	3 3 1
144.71	0.81	8	4 2 0

Table A.3 XRD data for copper oxide

Compound Name: Copper Oxide **Chemical Formula:** CuO **PDF Card No:** 00-041-0254 **Radiation:** $CuK_{\alpha 1}$ **Wavelength:** 1.5405 Å			
2θ (˚)	**d spacing (Å)**	**Intensity (%)**	**h k l**
32.51	2.75	8	1 1 0
35.44	2.53	60	0 0 2
35.54	2.52	100	-1 1 1
38.73	2.32	100	1 1 1
38.94	2.31	100	2 0 0
46.26	1.96	3	-1 1 2
48.74	1.87	25	-2 0 2
53.46	1.71	7	0 2 0
58.31	1.58	12	2 0 2
61.55	1.50	16	-1 1 3
65.82	1.42	12	0 2 2
66.27	1.41	14	-3 1 1
67.93	1.38	9	1 1 3
68.14	1.37	14	2 2 0
72.43	1.30	6	3 1 1
74.99	1.26	6	0 0 4
75.26	1.26	7	-2 2 2
80.19	1.20	2	-2 0 4
82.37	1.17	4	-3 1 3
83.10	1.16	4	2 2 2
83.68	1.15	4	4 0 0
86.57	1.12	2	-4 0 2
89.81	1.09	5	-1 3 1

Table A.4 XRD data for copper oxide

Compound Name: Copper Oxide **Chemical Formula:** Cu_2O **PDF Card No:** 00-005-0667 **Radiation:** $CuK_{\alpha 1}$ **Wavelength:** 1.5405 Å			
2θ (°)	**d spacing (Å)**	**Intensity (%)**	**h k l**
29.55	3.02	9	1 1 0
36.42	2.46	100	1 1 1
42.30	2.13	37	2 0 0
52.45	1.74	1	2 1 1
61.34	1.51	27	2 2 0
69.57	1.35	1	3 1 0
73.53	1.29	17	3 1 1
77.32	1.23	4	2 2 2
92.38	1.07	2	4 0 0
103.70	0.98	4	3 3 1
107.56	0.95	3	4 2 0
124.22	0.87	3	4 2 2
139.28	0.82	3	5 1 1

Table A.5 XRD data for zinc

Compound Name: Zinc **Chemical Formula:** Zn **PDF Card No:** 00-004-0831 **Radiation:** $CuK_{\alpha 1}$ **Wavelength:** 1.5405 Å			
2θ (°)	**d spacing (Å)**	**Intensity (%)**	**h k l**
36.30	2.47	53	0 0 2
39.99	2.31	40	1 0 0
43.23	2.09	100	1 0 1
54.33	1.69	28	1 0 2
70.06	1.34	25	1 0 3
70.66	1.33	21	1 1 0
77.03	1.24	2	0 0 4
82.10	1.17	23	1 1 2
83.76	1.15	5	2 0 0
86.56	1.12	17	2 0 1
89.92	1.09	3	1 0 4
94.90	1.04	5	2 0 2
109.13	0.94	8	2 0 3
115.80	0.91	6	1 0 5
116.38	0.91	11	1 1 4
124.05	0.87	5	2 1 0
127.49	0.86	9	2 1 1
131.84	0.84	2	2 0 4
138.21	0.82	1	0 0 6
138.95	0.82	9	2 1 2

Table A.6 XRD data for zinc oxide

Compound Name: Zinc Oxide **Chemical Formula:** ZnO **PDF Card No:** 00-036-1451 **Radiation:** $CuK_{\alpha 1}$ **Wavelength:** 1.5405 Å			
2θ (°)	**d spacing (Å)**	**Intensity (%)**	**h k l**
31.77	2.81	57	1 0 0
34.42	2.60	44	0 0 2
36.25	2.47	100	1 0 1
47.54	1.91	23	1 0 2
56.60	1.62	32	1 1 0
62.86	1.48	29	1 0 3
66.38	1.41	4	2 0 0
67.96	1.38	23	1 1 2
69.10	1.36	11	2 0 1
72.56	1.30	2	0 0 4
76.95	1.24	4	2 0 2
81.37	1.18	1	1 0 4
89.60	1.09	7	2 0 3
92.78	1.06	3	2 1 0
95.30	1.04	6	2 1 1
98.61	1.01	4	1 1 4
102.94	0.98	2	2 1 2
104.13	0.98	5	1 0 5
110.39	0.94	3	3 0 0
116.27	0.91	8	2 1 3
121.57	0.88	4	3 0 2
133.92	0.84	3	2 0 5
138.50	0.82	2	2 1 4
142.91	0.81	3	2 2 0

B. GC Calibration

GC calibration factor calculations were made via Gay-Lussac's Law. At the same temperature and pressure, assuming that the gases conform to the ideal gas, the gas volumes are proportional to the number of moles of the gases.

The CO calibration factor (β_{CO}) was taken as 1, and the calibration factor (β) for each component (i) was calculated from the formula below.

$$\frac{n_{CO}}{n_i} = \frac{A_{CO} \times \beta_{CO}}{A_i \times \beta_i}$$

where β_{CO} is the calibration factor of CO, n_{CO} is the number of moles of CO, and A_{CO} is the area under the CO peak in the GC pictogram

Table B.1 gives calibration factors for reactants and products that were seen in the reactor effluent stream.

Table B.1 Calibration factors for reactants and products

Component	Calibration Factor
CO	1.00
CO_2	0.85
CH_4	0.31
Methanol	1.70
DME	0.27
Ethanol	0.36
Formic acid	0.46
H_2	0.11

C. Conversion and Selectivity Calculations

To determine the amount of CO fed to the reactor ($n_{CO,0}$), a total carbon balance was performed, and the number of total carbon monoxide entering the system was calculated using equation C.1. All carbonaceous compounds originated from CO because CO was the only carbon source. Since there are two carbon atoms in DME and ethanol, their moles are multiplied by 2.

$$n_{CO,0} = n_{CO} + n_{CH_4} + n_{CO_2} + n_{MeOH} + 2 \times n_{DME} + n_{FA} + 2 \times n_{EtOH} \quad \text{(C.1)}$$

CO conversion was calculated from equation C.2.

$$X_{CO} = \frac{n_{CO,0} - n_{CO}}{n_{CO,0}} = \frac{n_{CH_4} + n_{CO_2} + n_{MeOH} + 2 \times n_{DME} + n_{FA} + 2 \times n_{EtOH}}{n_{CO} + n_{CH_4} + n_{CO_2} + n_{MeOH} + 2 \times n_{DME} + n_{FA} + 2 \times n_{EtOH}} \quad \text{(C.2)}$$

Equation C.3 was used to calculate the selectivity of CO_2, CH_4, formic acid, and methanol.

$$S_i = \frac{n_i}{n_{CO,0} - n_{CO}} = \frac{n_i}{n_{CH_4} + n_{CO_2} + n_{MeOH} + 2 \times n_{DME} + n_{FA} + 2 \times n_{EtOH}} \quad \text{(C.3)}$$

Equation C.4 was used to calculate the selectivity of DME and ethanol.

$$S_i = \frac{2 \times n_i}{n_{CO,0} - n_{CO}} = \frac{2 \times n_i}{n_{CH_4} + n_{CO_2} + n_{MeOH} + 2 \times n_{DME} + n_{FA} + 2 \times n_{EtOH}} \quad \text{(C.4)}$$

Yields were calculated from equation C.5.

$$Y_i = S_i \times X_i \quad \text{(C.5)}$$